Karlsruhe Institute of Technology

Wave phenomena
analysis and numerics

Parallel adaptive discontinuous Galerkin discretizations in space and time for linear elastic and acoustic waves

Willy Dörfler, Stefan Findeisen,
Christian Wieners, Daniel Ziegler

CRC Preprint 2018/14, August 2018

KARLSRUHE INSTITUTE OF TECHNOLOGY

CRC 1173

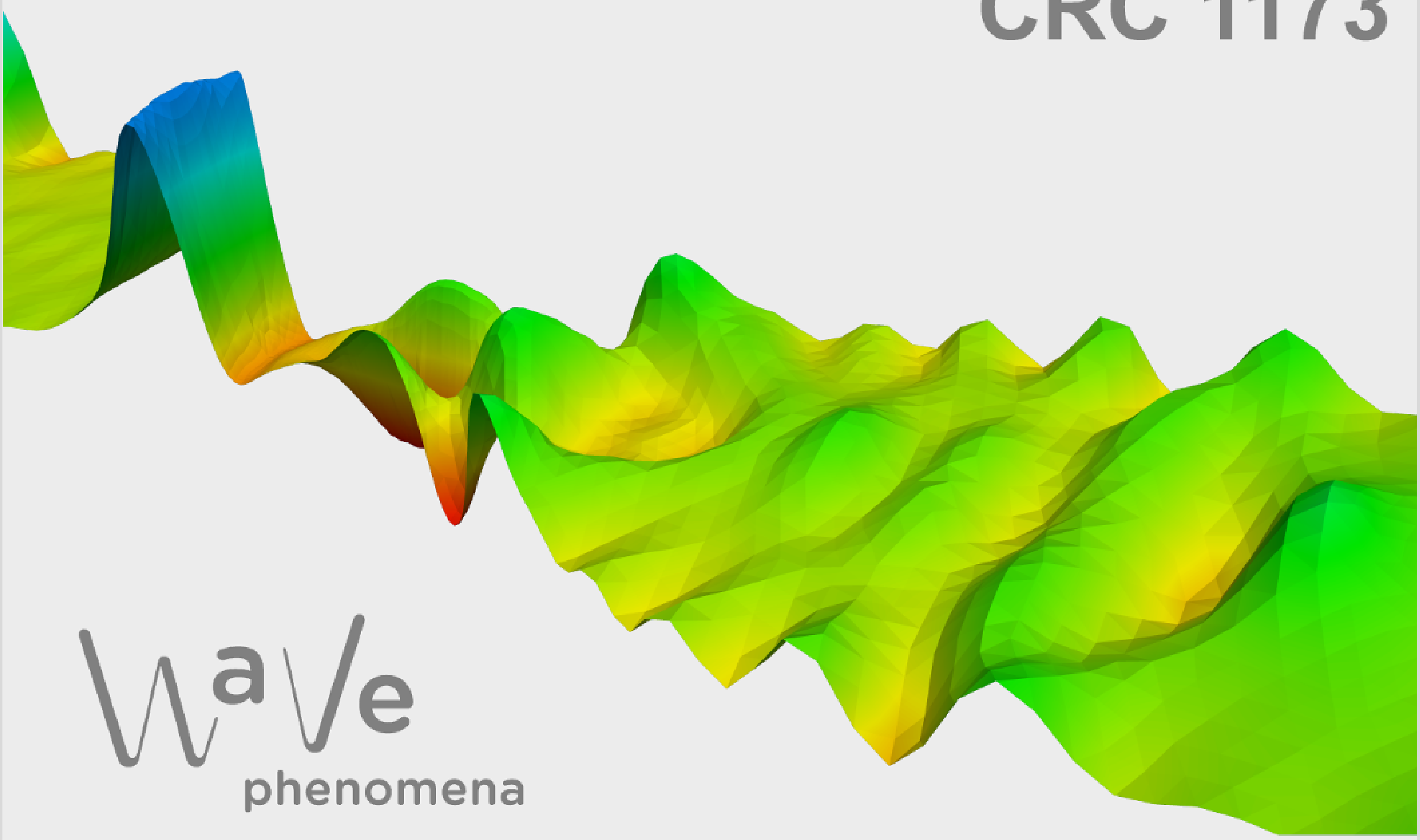

Participating universities

Universität Stuttgart

EBERHARD KARLS
UNIVERSITÄT
TÜBINGEN

Funded by

DFG

ISSN 2365-662X

XXXX, 1–29

Parallel adaptive discontinuous Galerkin discretizations in space and time for linear elastic and acoustic waves

Willy Dörfler, Stefan Findeisen, Christian Wieners and Daniel Ziegler

Abstract. We introduce a space-time discretization for elastic and acoustic waves using a discontinuous Galerkin approximation in space and a Petrov–Galerkin scheme in time. For the dG method, the upwind flux is evaluated by explicitly solving a Riemann problem. Then we show well-posedness and convergence of the discrete system. Based on goal-oriented dual-weighted error estimation an adaptive strategy is introduced. The full space-time linear system is solved with a parallel multilevel preconditioner. Numerical experiments for acoustic and elastic waves underline the efficiency of the overall adaptive solution process.

Keywords. Space-time methods, discontinuous Galerkin finite elements, linear hyperbolic systems, elastic and acoustic wave equation, dual weighted residual error estimator.

AMS classification. 65N30.

1 Introduction

Modern discretizations of time-dependent PDEs consider the full problem in the space-time cylinder and aim to overcome limitations of classical approaches such as the method of lines (first discretize in space and then solve the resulting ODE) and the Rothe method (first discretize in time and then solve the PDE). A main advantage of a holistic space-time method is the direct access to space-time adaptivity and to the backward problem (required for the goad-oriented error control or the dual problem in optimization, see [13] for more details). Moreover, this allows for parallel solution strategies simultaneously in time and space.

Several space-time concepts were proposed (different conforming and non-conforming space-time finite elements [34, 10, 23, 21, 33, 31, 36, 24, 28], the parareal method [25, 18], wavefront relaxation [16] etc.) and this topic has become an rapidly growing field in numerical analysis and scientific computing.

A further motivation for developing space-time methods is the design of modern computer facilities with an enormous number of processor cores, where the parallel realization of conventional methods becomes inefficient. Since these machines allow a fully implicit space-time approach, new parallel solution techniques are required to solve the huge linear systems, particularly for time-dependent applications in three

We gratefully acknowledge the support of the German Research Foundation (DFG) by CRC 1173.

spatial dimensions. Iterative solution techniques for full space-time discretizations were investigated, e.g., in [15, 29, 5, 35, 1, 2, 14, 38, 17, 37].

Here, we use in space a discontinuous Galerkin (DG) method for time-dependent first-order systems, see, e.g., [19], where this discretization is coupled with explicit time integration. This is applied to acoustic and elastic waves in [9] in combination with an adaptive space-time hp-strategy. We then extend these spatial DG discretization by a Petrov–Galerkin method in time with continuous ansatz space and discontinuous test space (cf. [3] for the implicit midpoint rule). The second-order formulation in space for elastic waves with implicit discontinuous Galerkin time discretization is considered in [22].

The DG approach uses the same variational space-time setting as discontinuous Petrov–Galerkin (DPG) methods for general linear first-order systems in space and time, see [6] for an overview and [11, 7] for space-time applications. For acoustic and elastic waves, the hybridization in space (applied to the second-order formulation) is presented in [30], and a hybrid space-time discontinuous Galerkin method is proposed in [39]. Both methods are implicit in every time slab, and only Dirichlet traces are used for the hybrid coupling. Space-time (Trefftz) discontinuous Galerkin methods for wave problems are analyzed in [10, 23].

Error estimation for linear wave equations require a backtracking of the error source as it is provided by a dual-primal error estimator. This achieves a reliable error control by solving the adjoint problem together with a goal-oriented technique [3].

Here we transfer our results for the linear transport equation and for the Maxwell system in [8] to acoustic and elastic waves. We start with an introduction of the first-order system for the wave equation and a suitable variational setting which provides stability of the space-time operator in a Hilbert space setting. Then we review the construction of discontinuous Galerkin methods for linear systems of conservation laws, and we compute the numerical flux for acoustic and elastic waves by solving the corresponding Riemann problem. In the next section we derive an explicit error representation (involving the solution of the dual problem), where we extend our approach in [8] by a different variant to estimate the interpolation error of the dual problem which can be estimated without additional regularity assumptions. We shortly summarize the construction of a suitable space-time multigrid preconditioner for the fully coupled implicit space-time discretization. Finally, the convergence of the method and the efficiency of the adaptive strategy is demonstrated for examples comparing the propagation of acoustic and elastic waves.

2 Linear elastic and acoustic waves

The prototype equation describing linear waves in homogeneous media is the second-order evolution equation for a scalar potential ϕ

$$\partial_t^2 \phi = \Delta \phi$$

subject to initial and boundary conditions. Introducing the pressure $p = \partial_t \phi$ and the velocity $\mathbf{v} = \nabla \phi$, we obtain the first-order system

$$\partial_t p = \nabla \cdot \mathbf{v} \,,$$
$$\partial_t \mathbf{v} = \nabla p$$

describing, e.g., acoustic waves. This system is now extended to describe linear elastic waves.

Waves in solids Let $\Omega \subseteq \mathbb{R}^D$ be a bounded Lipschitz domain, and let $[0,T]$ be a finite time interval. In dynamic models in continuum mechanics, the motion of a material point $\mathbf{x}$ in the reference configuration Ω at time t is described by the deformation vector $\boldsymbol{\varphi}(t,\mathbf{x})$. The velocity is denoted by $\mathbf{v} = \partial_t \boldsymbol{\varphi}$. Elastic waves are determined by Newton's law for the balance of momentum

$$\rho \partial_t \mathbf{v} = \operatorname{div} \boldsymbol{\sigma} + \mathbf{b} \,,$$

with the mass density ρ, acceleration $\partial_t \mathbf{v}$, and the vector of body forces $\mathbf{b}$, together with a constitutive relation for the stress $\boldsymbol{\sigma}$ depending on the deformation gradient $\mathbf{F} = \mathrm{D}\boldsymbol{\varphi}$. For elastic materials a response function $\hat{\Sigma}(\cdot)$ exists so that the stress is determined by the response $\boldsymbol{\sigma} = \hat{\Sigma}(\mathbf{F})$. Then the stress rate is given by

$$\partial_t \boldsymbol{\sigma} = \mathrm{D}\hat{\Sigma}(\mathrm{D}\boldsymbol{\varphi})(\mathrm{D}\mathbf{v}) \,.$$

Assuming small strains and $\boldsymbol{\varphi} \approx \mathrm{id}$, this is approximated by its linearization

$$\partial_t \boldsymbol{\sigma} = \mathbf{C}\boldsymbol{\varepsilon}(\mathbf{v}) \,, \qquad \boldsymbol{\varepsilon}(\mathbf{v}) = \operatorname{sym}(\mathrm{D}\mathbf{v})$$

with the elasticity tensor $\mathbf{C} = \mathrm{D}\hat{\Sigma}(\mathbf{I})$. The balance of torsional moments yields that the stress is symmetric and that the stress rate only depends on the symmetric strain rate. In isotropic media the elasticity tensor $\mathbf{C}\boldsymbol{\varepsilon} = 2\mu\boldsymbol{\varepsilon} + \lambda \operatorname{trace}(\boldsymbol{\varepsilon})\mathbf{I}$ is characterized by the Lamé parameters $\lambda \geq 0$, $\mu > 0$. Introducing the compression modulus $\kappa = \frac{2\mu+3\lambda}{3}$ and the deviatoric stress $\operatorname{dev}(\boldsymbol{\sigma}) = \boldsymbol{\sigma} - \frac{1}{3}\operatorname{trace}(\boldsymbol{\sigma})\mathbf{I}$ we obtain

$$\mathbf{C}\boldsymbol{\varepsilon} = 2\mu \operatorname{dev}(\boldsymbol{\varepsilon}) + \kappa \operatorname{trace}(\boldsymbol{\varepsilon})\mathbf{I} \,, \qquad \mathbf{C}^{-1}\boldsymbol{\sigma} = \frac{1}{2\mu}\operatorname{dev}(\boldsymbol{\sigma}) + \frac{1}{3\kappa}\operatorname{trace}(\boldsymbol{\sigma})\mathbf{I} \,.$$

Elastic Waves		*Acoustic Waves*	
$\partial_t\boldsymbol{\sigma} = \mathbf{C}\boldsymbol{\varepsilon}(\mathbf{v})$	in $(0,T)\times\Omega$	$\partial_t p = \kappa\,\mathrm{div}\,\mathbf{v}$	in $(0,T)\times\Omega$
$\rho\partial_t\mathbf{v} = \mathrm{div}\,\boldsymbol{\sigma} + \mathbf{b}$	in $(0,T)\times\Omega$	$\rho\partial_t\mathbf{v} = \nabla p + \mathbf{b}$	in $(0,T)\times\Omega$
$\boldsymbol{\sigma}(0) = \boldsymbol{\sigma}_0$	at $t=0$ in Ω	$p(0) = p_0$	at $t=0$ in Ω
$\mathbf{v}(0) = \mathbf{v}_0$	at $t=0$ in Ω	$\mathbf{v}(0) = \mathbf{v}_0$	at $t=0$ in Ω
$\boldsymbol{\sigma}\mathbf{n} = \mathbf{t}_{\mathrm{stat}}$	on $(0,T)\times\Gamma_{\mathrm{stat}}$	$p = p_{\mathrm{stat}}$	on $(0,T)\times\Gamma_{\mathrm{stat}}$
$\mathbf{v} = \mathbf{g}_{\mathrm{kin}}$	on $(0,T)\times\Gamma_{\mathrm{kin}}$	$\mathbf{n}\cdot\mathbf{v} = g_{\mathrm{kin}}$	on $(0,T)\times\Gamma_{\mathrm{kin}}$

Table 1. First-order differential systems for elastic waves in $(0,T)\times\Omega$ with initial conditions at $t=0$, and static and kinematic boundary conditions on $\partial\Omega = \Gamma_{\mathrm{stat}}\cup\Gamma_{\mathrm{kin}}$.

Acoustic waves in fluids In fluids we assume that shear forces can be neglected, i.e., we consider the limit $\mu\to 0$. Then, the stress $\boldsymbol{\sigma} = p\mathbf{I}$ is isotropic with hydrostatic pressure $p = \frac{1}{3}\,\mathrm{trace}\,\boldsymbol{\sigma}$, and compression waves are described by the system

$$\partial_t p = \kappa\,\mathrm{div}\,\mathbf{v}\,, \qquad \rho\partial_t\mathbf{v} = \nabla p + \mathbf{b}\,.$$

In particular this applies to acoustic waves in air or in a gas at fixed temperature. Note that this is only a formal derivation of the acoustic wave equation using the setting of continuum mechanics of solids, see Table 1 for comparing the elastic and acoustic setting. The linearization of conservation laws for compressible fluids with a pressure-dependent constitutive relation for the density results in the same system for acoustic waves.

First-order differential systems The previous examples are instances of a system of J equations in $\mathbb{R}^D$

$$M\partial_t\mathbf{u} + A\mathbf{u} = \mathbf{f},$$

with a first order differential operator A and a weighting operator M, see Table 2.

We introduce the Hilbert space $H = \mathrm{L}_2(\Omega;\mathbb{R}^J)$ with weighted inner product

$$(\mathbf{v},\mathbf{w})_H = (M\mathbf{v},\mathbf{w})_{0,\Omega}\,,$$

where we assume that the operator $M\in\mathrm{L}_\infty(\Omega,\mathbb{R}^{J\times J}_{\mathrm{sym}})$ is uniformly positive. The analysis of the wave problems will be considered with homogeneous boundary conditions on $\partial\Omega$ which are realized by the choice of a suitable domain $\mathcal{D}(A)\subset H$. We assume that the operator A is skew-adjoint in the domain, i.e.,

$$(A\mathbf{v},\mathbf{w})_{0,\Omega} = -(\mathbf{v},A\mathbf{w})_{0,\Omega} \qquad \mathbf{v},\mathbf{w}\in\mathcal{D}(A)\,. \tag{2.1}$$

For the corresponding evolution operator $L = M\partial_t + A$ on the space-time cylinder $Q = (0,T)\times\Omega$ we also observe

$$(L\mathbf{v},\mathbf{w})_{0,Q} = -(\mathbf{v},L\mathbf{w})_{0,Q}\,, \qquad \mathbf{v},\mathbf{w}\in\mathrm{C}^1_{\mathrm{c}}(Q;\mathbb{R}^J)\,,$$

Elastic Waves	*Acoustic Waves*
$\mathbf{u} = (\boldsymbol{\sigma}, \mathbf{v})$	$\mathbf{u} = (p, \mathbf{v})$
$M(\boldsymbol{\sigma}, \mathbf{v}) = (\mathbf{C}^{-1}\boldsymbol{\sigma}, \rho\mathbf{v})$	$M(p, \mathbf{v}) = (\kappa^{-1}p, \rho\mathbf{v})$
$A(\boldsymbol{\sigma}, \mathbf{v}) = -(\varepsilon(\mathbf{v}), \operatorname{div}\boldsymbol{\sigma})$	$A(p, \mathbf{v}) = -(\operatorname{div}\mathbf{v}, \nabla p)$
$\mathbf{f} = (\mathbf{0}, \mathbf{b})$	$\mathbf{f} = (0, \mathbf{b})$
$\mathcal{D}(A) = \mathrm{H}(\mathrm{div}, \Omega; \mathbb{R}^{D\times D}_{\mathrm{sym}}) \times \mathrm{H}^1_0(\Omega; \mathbb{R}^D)$	$\mathcal{D}(A) = \mathrm{H}^1(\Omega) \times \mathrm{H}_0(\mathrm{div}, \Omega)$

Table 2. First-order differential systems $M\partial_t\mathbf{u} + A\mathbf{u} = \mathbf{f}$ and suitable domains $\mathcal{D}(A)$ for linear waves. Here, we choose kinematic boundary conditions (Dirichlet b.c. for elastic waves and Neumann b.c. for acoustic waves).

where C^1_c denotes the set of compactly supported differentiable mappings.

Depending on L we define the space

$$\mathrm{H}(L, Q) = \big\{\mathbf{v} \in \mathrm{L}_2(Q; \mathbb{R}^J) \colon \mathbf{g} \in \mathrm{L}_2(Q; \mathbb{R}^J) \text{ exists with } \\ (\mathbf{g}, \mathbf{w})_{0,Q} = -(\mathbf{v}, L\mathbf{w})_{0,Q} \text{ for all } \mathbf{w} \in \mathrm{C}^1_\mathrm{c}(Q; \mathbb{R}^J)\big\} .$$

Then, L can be extended to this space, and $\mathrm{H}(L, \Omega)$ is a Hilbert space with respect to the weighted graph norm $\|\mathbf{v}\|_{L,Q} = \sqrt{(Mv, v)^2_{0,Q} + (M^{-1}L\mathbf{v}, L\mathbf{v})^2_{0,Q}}$.

Let $V \subset \mathrm{H}(L, Q)$ be the closure of $\big\{\mathbf{v} \in \mathrm{C}^1([0, T]; \mathcal{D}(A)) \colon \mathbf{v}(0) = \mathbf{0}\big\}$ with respect to the graph norm. In particular, the space V includes homogeneous initial conditions. Then we define $W = \overline{L(V)} \subseteq \mathrm{L}_2(Q; \mathbb{R}^J)$ with the weighted norm $\|\mathbf{w}\|^2_W = (M\mathbf{w}, \mathbf{w})_{0,Q}$. On V, we use the weighted graph norm $\|\mathbf{v}\|^2_V = \|\mathbf{v}\|^2_W + \|M^{-1}L\mathbf{v}\|^2_W$.

Since A is skew-adjoint, we obtain the operator estimate in weighted norms [8, Lem. 1]

$$\|\mathbf{v}\|_W \le 2T\, \|M^{-1}L\mathbf{v}\|_W , \qquad \mathbf{v} \in V . \tag{2.2}$$

This implies that $L \in \mathcal{L}(V, W)$ is injective and the range is closed. Moreover, for $\mathbf{f} \in W$ a unique solution $\mathbf{u} \in V$ of the evolution equation

$$L\mathbf{u} = \mathbf{f} \tag{2.3}$$

exists [8, Lem. 2]. This extends to initial values $\mathbf{u}(0) = \mathbf{u}_0 \ne \mathbf{0}$ by replacing $\mathbf{f}(t)$ with $\mathbf{f}(t) - A\mathbf{u}_0$. Also inhomogeneous boundary conditions can be analyzed by modifying the right-hand side when the existence of a sufficiently smooth extension of the boundary data can be assumed.

Remark 2.1. Since L mixes the derivatives in space and time, more regularity is difficult to show in this Hilbert space framework. Therefore, one can check the assumptions of the Lumer–Phillips theorem [32, Thm. 12.22] for the operator A in $\mathcal{D}(A)$, so that semigroup theory with more regularity can be applied, see, e.g., [12]. The application to wave equations is discussed in [20, Sect. 2.2].

3 Discontinuous Galerkin methods for linear systems of conservation laws

All wave equations discussed so far can be more specifically considered as a system of linear conservation laws

$$M\partial_t \mathbf{u}(t) + \operatorname{div} \mathbf{F}(\mathbf{u}(t)) = \mathbf{f}(t) \quad \text{for } t \in [0,T]\,, \qquad \mathbf{u}(0) = \mathbf{u}_0\,, \tag{3.1}$$

with a linear *flux function* $\mathbf{F}(\mathbf{v}) = [B_1\mathbf{v}, \dots, B_D\mathbf{v}]$ defined by symmetric matrices $B_d \in \mathbb{R}^{J\times J}_{\text{sym}}$ such that

$$A\mathbf{v} = \operatorname{div} \mathbf{F}(\mathbf{v}) = \sum_{d=1}^{D} B_d \partial_d \mathbf{v}\,.$$

Traveling waves In the case of constant coefficients in $\Omega = \mathbb{R}^D$, special solutions can be constructed as follows. For a given unit vector $\mathbf{n} = (n_1, \dots, n_D)^\top \in \mathbb{R}^D$, we have $\mathbf{n}\cdot\mathbf{F}(\mathbf{u}) = B_\mathbf{n}\mathbf{u}$ with the symmetric matrix $B_\mathbf{n} = \sum_{d=1}^D n_d B_d$. Then, for all eigenpairs $(\lambda, \mathbf{w}) \in \mathbb{R}\times\mathbb{R}^J$ of $B_\mathbf{n}\mathbf{w} = \lambda M\mathbf{w}$ and all sufficiently smooth functions $a\colon \mathbb{R}\to\mathbb{R}$, the traveling wave propagating with velocity $c = |\lambda|$

$$\mathbf{u}(t,\mathbf{x}) = a(\mathbf{n}\cdot\mathbf{x} - \lambda t)\,\mathbf{w}$$

is a solution of (3.1) with initial value $\mathbf{u}_0(\mathbf{x}) = a(\mathbf{n}\cdot\mathbf{x})\,\mathbf{w}$ and right-hand side $\mathbf{f} = \mathbf{0}$.

This also applies to traveling waves with discontinuous amplitude: the piecewise constant function

$$\mathbf{u}(t,\mathbf{x}) = \begin{cases} a_\text{L}\mathbf{w} & \text{in } Q_\text{L} = \big\{(t,\mathbf{x}) \in [0,T]\times\mathbb{R}^D \colon \mathbf{n}\cdot\mathbf{x} - \lambda t < 0\big\}, \\ a_\text{R}\mathbf{w} & \text{in } Q_\text{R} = \big\{(t,\mathbf{x}) \in [0,T]\times\mathbb{R}^D \colon \mathbf{n}\cdot\mathbf{x} - \lambda t > 0\big\}, \end{cases} \tag{3.2}$$

with $a_\text{L}, a_\text{R} \in \mathbb{R}$ is a weak solution, i.e., we have $\int_\mathbb{R}\int_{\mathbb{R}^D} \mathbf{u}\cdot L\mathbf{v}\,\mathrm{d}\mathbf{x}\mathrm{d}t = 0$ for all $\mathbf{v} \in \mathrm{C}^1_\text{c}(\mathbb{R}\times\mathbb{R}^D;\mathbb{R}^J)$.

The Riemann problem for linear conservation laws We now construct a weak solution of the *Riemann problem*, i.e., a piecewise constant weak solution with right-hand side $\mathbf{f} = \mathbf{0}$ and the discontinuous initial function

$$\mathbf{u}_0(\mathbf{x}) = \begin{cases} \mathbf{u}_\text{L} & \text{in } \Omega_\text{L} = \big\{\mathbf{x}\in\mathbb{R}^D \colon \mathbf{n}\cdot\mathbf{x} < 0\big\}, \\ \mathbf{u}_\text{R} & \text{in } \Omega_\text{R} = \big\{\mathbf{x}\in\mathbb{R}^D \colon \mathbf{n}\cdot\mathbf{x} > 0\big\}, \end{cases} \tag{3.3}$$

with $\mathbf{u}_\text{L}, \mathbf{u}_\text{R} \in \mathbb{R}^J$. Let $\{(\lambda_j, \mathbf{w}_j)\}_{j=1,\dots,J}$ be the (necessarily M-orthogonal) set of eigenpairs, i.e.,

$$B_\mathbf{n}\mathbf{w}_j = \lambda_j M\mathbf{w}_j \quad \text{with} \quad \mathbf{w}_k\cdot M\mathbf{w}_j = 0 \quad \text{for } j \neq k\,. \tag{3.4}$$

This defines a decomposition $B_{\mathbf{n}} = B_{\mathbf{n}}^- + B_{\mathbf{n}}^+$ with

$$B_{\mathbf{n}}^-\mathbf{v} = \sum_{\lambda_j<0} \lambda_j \frac{\mathbf{w}_j \cdot M\mathbf{v}}{\mathbf{w}_j \cdot M\mathbf{w}_j} M\mathbf{w}_j\,, \qquad B_{\mathbf{n}}^+\mathbf{v} = \sum_{\lambda_j>0} \lambda_j \frac{\mathbf{w}_j \cdot M\mathbf{v}}{\mathbf{w}_j \cdot M\mathbf{w}_j} M\mathbf{w}_j\,.$$

By superposition of traveling waves, we obtain a weak solution of the Riemann problem

$$\mathbf{u}(t,\mathbf{x}) = \sum_{j=1}^{J} a_j(\mathbf{x}\cdot\mathbf{n} - \lambda_j t)\mathbf{w}_j\,, \quad a_j(s) = \begin{cases} \dfrac{\mathbf{w}_j \cdot M\mathbf{u}_{\mathrm{L}}}{\mathbf{w}_j \cdot M\mathbf{w}_j} & s<0\,, \\[2ex] \dfrac{\mathbf{w}_j \cdot M\mathbf{u}_{\mathrm{R}}}{\mathbf{w}_j \cdot M\mathbf{w}_j} & s>0\,. \end{cases}$$

The solution of the Riemann problem at $(t,\mathbf{0})$ for $t>0$ defines the upwind flux on the interface $\partial\Omega_{\mathrm{L}} \cap \partial\Omega_{\mathrm{R}}$ by

$$\begin{aligned} \mathbf{n}\cdot\mathbf{F}^{\mathrm{num}}(\mathbf{u}_0) &= \sum_{\lambda_j>0} \frac{\mathbf{w}_j \cdot M\mathbf{u}_{\mathrm{L}}}{\mathbf{w}_j \cdot M\mathbf{w}_j} B_{\mathbf{n}}\mathbf{w}_j + \sum_{\lambda_j<0} \frac{\mathbf{w}_j \cdot M\mathbf{u}_{\mathrm{R}}}{\mathbf{w}_j \cdot M\mathbf{w}_j} B_{\mathbf{n}}\mathbf{w}_j \\ &= B_{\mathbf{n}}\mathbf{u}_{\mathrm{L}} + B_{\mathbf{n}}^-[\mathbf{u}] \end{aligned} \tag{3.5}$$

depending on the jump term $[\mathbf{u}] = \mathbf{u}_{\mathrm{R}} - \mathbf{u}_{\mathrm{L}}$. By construction, the upwind flux is consistent, i.e., for $B_{\mathbf{n}}\mathbf{u}_{\mathrm{L}} = B_{\mathbf{n}}\mathbf{u}_{\mathrm{R}}$ we obtain $\mathbf{n}\cdot\mathbf{F}^{\mathrm{num}}(\mathbf{u}_0) = B_{\mathbf{n}}\mathbf{u}_{\mathrm{L}} = B_{\mathbf{n}}\mathbf{u}_{\mathrm{R}}$.

This transfers to the solution of the Riemann problem and the evaluation of the numerical flux in case of different material parameters in Ω_{L} and Ω_{R}, i.e., two different matrices M_{L} and M_{R}; see [20, Sect. 3.2] for details.

Application to wave equations For *elastic waves* with $\operatorname{div}\mathbf{F}(\boldsymbol{\sigma},\mathbf{v}) = -(\varepsilon(\mathbf{v}), \operatorname{div}\boldsymbol{\sigma})$ we have the normal flux

$$\mathbf{n}\cdot\mathbf{F}(\boldsymbol{\sigma},\mathbf{v}) = -\begin{pmatrix} \frac12(\mathbf{n}\otimes\mathbf{v} + \mathbf{v}\otimes\mathbf{n}) \\ \boldsymbol{\sigma}\mathbf{n} \end{pmatrix}.$$

Now we consider the isotropic case, where $c_{\mathrm{P}} = \sqrt{(2\mu+\lambda)/\rho}$ is the velocity of pressure waves, and $c_{\mathrm{S}} = \sqrt{\mu/\rho}$ is the velocity of shear waves. The eigenvalues in (3.4) are $\pm c_{\mathrm{P}}$, $\pm c_{\mathrm{S}}$, and the corresponding eigenvectors are of the form $\begin{pmatrix} 2\mu\mathbf{n}\otimes\mathbf{n} + \lambda\mathbf{I} \\ \pm c_{\mathrm{P}}\mathbf{n} \end{pmatrix}$ and $\begin{pmatrix} \mu(\boldsymbol{\tau}\otimes\mathbf{n} + \mathbf{n}\otimes\boldsymbol{\tau}) \\ \pm c_{\mathrm{S}}\boldsymbol{\tau} \end{pmatrix}$, where $\boldsymbol{\tau}$ is a unit tangent vector, i.e., $\boldsymbol{\tau}\cdot\mathbf{n} = 0$. This yields

$$\begin{aligned} B_{\mathbf{n}}^-[\mathbf{u}] &= -\frac{\mathbf{n}\otimes\mathbf{n}\,[\boldsymbol{\sigma}] + \rho c_{\mathrm{P}}\mathbf{n}\cdot[\mathbf{v}]}{2\rho c_{\mathrm{P}}} \begin{pmatrix} \mathbf{n}\otimes\mathbf{n} \\ \rho c_{\mathrm{P}}\mathbf{n} \end{pmatrix} \\ &\quad -\frac{\frac12(\boldsymbol{\tau}\otimes\mathbf{n} + \mathbf{n}\otimes\boldsymbol{\tau})[\boldsymbol{\sigma}] + \rho c_{\mathrm{S}}\boldsymbol{\tau}\cdot[\mathbf{v}]}{2\rho c_{\mathrm{S}}} \begin{pmatrix} \frac12(\boldsymbol{\tau}\otimes\mathbf{n} + \mathbf{n}\otimes\boldsymbol{\tau}) \\ \rho c_{\mathrm{S}}\boldsymbol{\tau} \end{pmatrix}, \end{aligned}$$

and inserting (3.5) results in the 2D upwind flux

$$\mathbf{n}\cdot\mathbf{F}^{\mathrm{num}}(\mathbf{u}_0) = -\begin{pmatrix}\frac{1}{2}(\mathbf{n}\otimes\mathbf{v}_{\mathrm{L}}+\mathbf{v}_{\mathrm{L}}\otimes\mathbf{n})\\ \boldsymbol{\sigma}_{\mathrm{L}}\mathbf{n}\end{pmatrix} - \frac{\mathbf{n}\cdot[\boldsymbol{\sigma}]\mathbf{n}+\rho c_{\mathrm{P}}[\mathbf{v}]\cdot\mathbf{n}}{2\rho c_{\mathrm{P}}}\begin{pmatrix}\mathbf{n}\otimes\mathbf{n}\\ \rho c_{\mathrm{P}}\mathbf{n}\end{pmatrix}$$
$$- \frac{\boldsymbol{\tau}\cdot[\boldsymbol{\sigma}]\mathbf{n}+\rho c_{\mathrm{S}}[\mathbf{v}]\cdot\boldsymbol{\tau}}{2\rho c_{\mathrm{S}}}\begin{pmatrix}\frac{1}{2}(\boldsymbol{\tau}\otimes\mathbf{n}+\mathbf{n}\otimes\boldsymbol{\tau})\\ \rho c_{\mathrm{S}}\boldsymbol{\tau}\end{pmatrix}.$$

For *acoustic waves* with $\operatorname{div}\mathbf{F}(p,\mathbf{v}) = -(\operatorname{div}\mathbf{v},\nabla p)$ we obtain

$$\mathbf{n}\cdot\mathbf{F}(p,\mathbf{v}) = -\begin{pmatrix}\mathbf{n}\cdot\mathbf{v}\\ p\mathbf{n}\end{pmatrix},$$

the velocity of sound $c=\sqrt{\kappa/\rho}$, and the eigenvectors $\mathbf{w}_\pm = \begin{pmatrix}\kappa\\ \mp c\mathbf{n}\end{pmatrix}$.

This yields $B_{\mathbf{n}}^- = -\frac{1}{2}\begin{pmatrix}\frac{1}{\rho c} & \mathbf{n}\\ \mathbf{n} & \rho c\,\mathbf{n}\otimes\mathbf{n}\end{pmatrix}$ and thus the upwind flux

$$\mathbf{n}\cdot\mathbf{F}^{\mathrm{num}}(\mathbf{u}_0) \;=\; -\begin{pmatrix}\mathbf{n}\cdot\mathbf{v}_{\mathrm{L}}\\ p_{\mathrm{L}}\mathbf{n}\end{pmatrix} - \frac{[p]+\rho c\mathbf{n}\cdot[\mathbf{v}]}{2\rho c}\begin{pmatrix}1\\ \rho c\mathbf{n}\end{pmatrix}.$$

This extends to boundary conditions as follows.
For given values $(p_{\mathrm{L}},\mathbf{v}_{\mathrm{L}})$ the Riemann solution in Ω_L takes the form

$$\mathbf{u}(t,\mathbf{x}) = \begin{cases}\begin{pmatrix}p_{\mathrm{L}}\\ \mathbf{v}_{\mathrm{L}}\end{pmatrix} & \mathbf{x}\cdot\mathbf{n} < tc,\\ \begin{pmatrix}p_{\mathrm{L}}\\ \mathbf{v}_{\mathrm{L}}\end{pmatrix} + a\begin{pmatrix}\kappa\\ c\mathbf{n}\end{pmatrix} & \mathbf{x}\cdot\mathbf{n} > tc,\end{cases}$$

and the parameter a is determined by boundary conditions. For $p = p_{\mathrm{stat}}$ on $\partial\Omega_L$ we obtain $a = \dfrac{p_{\mathrm{stat}}-p_{\mathrm{L}}}{\kappa}$, and for $\mathbf{n}\cdot\mathbf{v} = g_{\mathrm{kin}}$ on $\partial\Omega_L$ we obtain $a = \dfrac{g_{\mathrm{kin}}-\mathbf{n}\cdot\mathbf{v}_{\mathrm{L}}}{c}$.
This yields on the boundary

$$\begin{aligned}\mathbf{n}\cdot\mathbf{F}^{\mathrm{num}}(\mathbf{u}) &= -\begin{pmatrix}\mathbf{n}\cdot\mathbf{v}_{\mathrm{L}}\\ p_{\mathrm{L}}\mathbf{n}\end{pmatrix} - c\frac{p_{\mathrm{stat}}-p_{\mathrm{L}}}{\kappa}\begin{pmatrix}1\\ \rho c\mathbf{n}\end{pmatrix}\\ &= -\begin{pmatrix}\mathbf{n}\cdot\mathbf{v}_{\mathrm{L}}\\ p_{\mathrm{L}}\mathbf{n}\end{pmatrix} - \frac{[p]+\rho c\mathbf{n}\cdot[\mathbf{v}]}{2\rho c}\begin{pmatrix}1\\ \rho c\mathbf{n}\end{pmatrix} - \frac{p_{\mathrm{stat}}}{\rho c}\begin{pmatrix}1\\ \rho c\mathbf{n}\end{pmatrix}\end{aligned}$$

with $[p] = -2p_{\mathrm{L}}$ and $\mathbf{n}\cdot[\mathbf{v}] = 0$ for the static case (Dirichlet b.c.), and

$$\begin{aligned}\mathbf{n}\cdot\mathbf{F}^{\mathrm{num}}(\mathbf{u}) &= -\begin{pmatrix}\mathbf{v}_{\mathrm{L}}\cdot\mathbf{n}\\ p_{\mathrm{L}}\mathbf{n}\end{pmatrix} - c\frac{g_{\mathrm{kin}}-\mathbf{n}\cdot\mathbf{v}_{\mathrm{L}}}{c}\begin{pmatrix}1\\ \rho c\mathbf{n}\end{pmatrix}\\ &= -\begin{pmatrix}\mathbf{v}_{\mathrm{L}}\cdot\mathbf{n}\\ p_{\mathrm{L}}\mathbf{n}\end{pmatrix} - \frac{[p]+\rho c\mathbf{n}\cdot[\mathbf{v}]}{2\rho c}\begin{pmatrix}1\\ \rho c\mathbf{n}\end{pmatrix} + g_{\mathrm{kin}}\begin{pmatrix}1\\ \rho c\mathbf{n}\end{pmatrix}\end{aligned}$$

with $[p] = 0$ and $\mathbf{n}\cdot[\mathbf{v}] = -2\mathbf{n}\cdot\mathbf{v}_{\mathrm{L}}$ for the kinematic case (Neumann b.c.).

The discontinuous Galerkin discretization in space We assume that Ω is a bounded polyhedral Lipschitz domain decomposed into a finite number of open elements $K \subset \Omega$ such that $\bar{\Omega} = \bigcup_{K \in \mathcal{K}} \bar{K}$, where $\mathcal{K}$ is the set of elements in space. Let $\mathcal{F}_K$ be the set of faces of $K \in \mathcal{K}$. For inner faces $f \in \mathcal{F}_K$ let K_f be the neighboring cell such that $f = \partial K \cap \partial K_f$, and let $\mathbf{n}_K$ be the outer unit normal vector on ∂K. The outer unit normal vector field on $\partial\Omega$ is denoted by $\mathbf{n}$.

We select polynomial degrees p_K, and define the local spaces $H_{h,K} = \mathbb{P}_{p_K}(K; \mathbb{R}^J)$ and the global discontinuous Galerkin space

$$H_h = \big\{ \mathbf{v}_h \in \mathrm{L}_2(\Omega)^J : \mathbf{v}_h|_K \in H_{h,K} \text{ for all } K \in \mathcal{K} \big\}.$$

For $\mathbf{v}_h \in H_h$ we define $\mathbf{v}_{h,K} = \mathbf{v}_h|_K \in H_{h,K}$ for the restriction to K. In the semi-discrete problem

$$M_h \partial_t \mathbf{u}_h(t) + A_h \mathbf{u}_h(t) = \mathbf{f}_h(t)\,, \qquad t \in (0,T)\,, \tag{3.6}$$

the discrete mass operator $M_h \in \mathcal{L}(H_h, H_h)$ and the right-hand side $\mathbf{f}_h \in H_h$ are the Galerkin approximations of M and $\mathbf{f}$ defined by

$$\begin{aligned} (M_h \mathbf{v}_h, \mathbf{w}_h)_{0,\Omega} &= (M \mathbf{v}_h, \mathbf{w}_h)_{0,\Omega} && \mathbf{v}_h, \mathbf{w}_h \in H_h\,, \\ (\mathbf{f}_h, \mathbf{w}_h)_{0,\Omega} &= (\mathbf{f}, \mathbf{w}_h)_{0,\Omega} && \mathbf{w}_h \in H_h\,. \end{aligned} \tag{3.7}$$

Note that M_h is represented by a block diagonal positive definite matrix.

The discrete operator $A_h \in \mathcal{L}(H_h, H_h)$ is constructed as follows: Integration by parts yields for smooth ansatz functions $\mathbf{v}$ and smooth test functions ϕ_K

$$\begin{aligned} (A\mathbf{v}, \phi_K)_{0,K} &= (\operatorname{div} \mathbf{F}(\mathbf{v}), \phi_K)_{0,K} \\ &= -(\mathbf{F}(\mathbf{v}), \nabla \phi_K)_{0,K} + \sum_{f \in \mathcal{F}_K} (\mathbf{n}_K \cdot \mathbf{F}(\mathbf{v}), \phi_K)_{0,f}\,. \end{aligned}$$

We then define for $\mathbf{v}_h \in H_h$ and $\phi_{h,K} \in H_{h,K}$

$$(A_h \mathbf{v}_h, \phi_{h,K})_{0,K} = -(\mathbf{F}(\mathbf{v}_{h,K}), \nabla \phi_{h,K})_{0,K} + \sum_{f \in \mathcal{F}_K} \big(\mathbf{n}_K \cdot \mathbf{F}_K^{\text{num}}(\mathbf{v}_h), \phi_{h,K} \big)_{0,f}\,,$$

where $\mathbf{n}_K \cdot \mathbf{F}_K^{\text{num}}(\mathbf{v}_h)$ is the upwind flux obtained from local solutions of Riemann problems. Again using integration by parts, we obtain

$$\begin{aligned} (A_h \mathbf{v}_h, \phi_{h,K})_{0,K} &= \big(\operatorname{div} \mathbf{F}(\mathbf{v}_{h,K}), \phi_{h,K} \big)_{0,K} \\ &\quad + \sum_{f \in \mathcal{F}_K} \big(\mathbf{n}_K \cdot (\mathbf{F}_K^{\text{num}}(\mathbf{v}_h) - \mathbf{F}(\mathbf{v}_{h,K})), \phi_{h,K} \big)_{0,f}\,. \end{aligned} \tag{3.8}$$

On inner faces $f = \partial K \cap \partial K_f$ the difference $\mathbf{n}_K \cdot (\mathbf{F}_K^{\text{num}}(\mathbf{v}_h) - \mathbf{F}(\mathbf{v}_{h,K}))$ only depends on the jump term $[\mathbf{v}_h]_{K,f} = \mathbf{v}_{h,K_f} - \mathbf{v}_{h,K}$, so that $\mathbf{n}_K \cdot (\mathbf{F}_K^{\text{num}}(\mathbf{v}) - \mathbf{F}(\mathbf{v})) = 0$ on all faces $f \in \mathcal{F}_K$ for $\mathbf{v} \in \mathcal{D}(A)$. On boundary faces, we define the jump term $[\mathbf{v}_h]_{K,f}$ depending on the boundary conditions as in the last paragraph. On H_h we define the operator A_h by

$$(A_h\mathbf{v}_h, \boldsymbol{\phi}_h)_{0,K} = \sum_{K\in\mathcal{K}} (A_h\mathbf{v}_h, \boldsymbol{\phi}_{h,K})_{0,K}\,, \qquad \mathbf{v}_h, \boldsymbol{\phi}_h \in H_h\,.$$

By construction, the operator A_h satisfies the consistency condition

$$(A\mathbf{v}, \boldsymbol{\phi}_h)_{0,\Omega} = (A_h\mathbf{v}, \boldsymbol{\phi}_h)_{0,\Omega}\,, \qquad \mathbf{v} \in \mathcal{D}(A)\,,\ \boldsymbol{\phi}_h \in H_h\,, \tag{3.9}$$

since the numerical flux $\mathbf{F}^{\mathrm{num}}$ satisfies

$$\sum_{K\in\mathcal{K}} \big(\mathbf{n}_K \cdot \mathbf{F}_K^{\mathrm{num}}(\mathbf{v}_{h,K}), \mathbf{v}\big)_{0,\partial K} = 0\,, \qquad \mathbf{v} \in \mathcal{D}(A) \cap \mathrm{H}^1(\Omega;\mathbb{R}^J) \tag{3.10}$$

for $\mathbf{v}_h \in H_h$. For our applications we can show that the upwind flux together with the described choice of the boundary flux guarantees that the discrete operator is non-negative and controls the nonconformity, i.e., a constant $C_{\mathrm{A}} > 0$ exists such that

$$(A_h\mathbf{v}_h, \mathbf{v}_h)_{0,\Omega} \geq C_{\mathrm{A}} \sum_{f\in\mathcal{F}_K} \big\|\mathbf{n}_K \cdot (\mathbf{F}_K^{\mathrm{num}}(\mathbf{v}_h) - \mathbf{F}(\mathbf{v}_{h,K}))\big\|_{0,f}^2 \geq 0 \tag{3.11}$$

for all $\mathbf{v}_h \in H_h$.

For *elastic waves* we obtain for $(\boldsymbol{\sigma}_h, \mathbf{v}_h) \in H_h$ and $(\boldsymbol{\varphi}_{K,h}, \boldsymbol{\psi}_{K,h}) \in H_{K,h}$

$$\begin{aligned}
\big(A_h(\boldsymbol{\sigma}_h, \mathbf{v}_h), (\boldsymbol{\varphi}_{K,h}, \boldsymbol{\psi}_{K,h})\big)_{0,K} &= -\big(\varepsilon(\mathbf{v}_{K,h}), \boldsymbol{\varphi}_{K,h}\big)_{0,K} - \big(\operatorname{div}\boldsymbol{\sigma}_{K,h}, \boldsymbol{\psi}_{K,h}\big)_{0,K} \\
&\quad -\frac{1}{2\rho c_{\mathrm{S}}} \sum_{f\in\mathcal{F}_K} \big(\mathbf{n}_K \times ([\boldsymbol{\sigma}_h]_{K,f}\mathbf{n}_K + \rho c_{\mathrm{S}}[\mathbf{v}_h]_{K,f}), \mathbf{n}_K \times (\boldsymbol{\varphi}_{K,h}\mathbf{n}_K + \rho c_{\mathrm{S}}\boldsymbol{\psi}_{K,h})\big)_{0,f} \\
&\quad -\frac{1}{2\rho c_{\mathrm{P}}} \sum_{f\in\mathcal{F}_K} \big(\mathbf{n}_K \cdot ([\boldsymbol{\sigma}_h]_{K,f}\mathbf{n}_K + \rho c_{\mathrm{P}}[\mathbf{v}_h]_{K,f}), \mathbf{n}_K \cdot (\boldsymbol{\varphi}_{K,h}\mathbf{n}_K + \rho c_{\mathrm{P}}\boldsymbol{\psi}_{K,h})\big)_{0,f}\,.
\end{aligned}$$

On boundary faces $f = \partial K \cap \partial\Omega$, we set $[\mathbf{v}_h]_{K,f} = -2\mathbf{v}_{K,h}$ and $[\boldsymbol{\sigma}_h]_{K,f} = \mathbf{0}$ for Dirichlet boundary conditions. This yields

$$\begin{aligned}
\big(A_h(\boldsymbol{\sigma}_h, \mathbf{v}_h), (\boldsymbol{\sigma}_{K,h}, \mathbf{v}_{K,h})\big)_{0,K} &= -\sum_{f\in\mathcal{F}_K} \big(\mathbf{v}_{K,h}, \boldsymbol{\sigma}_{K,h}\mathbf{n}_K\big)_{0,f} \\
&\quad -\frac{1}{2\rho c_{\mathrm{S}}} \sum_{f\in\mathcal{F}_K} \big(\mathbf{n}_K \times ([\boldsymbol{\sigma}]_{K,f}\mathbf{n}_K + \rho c_{\mathrm{S}}[\mathbf{v}]_{K,f}), \mathbf{n}_K \times (\boldsymbol{\sigma}_{K,h}\mathbf{n}_K + \rho c_{\mathrm{S}}\mathbf{v}_{K,h})\big)_{0,f} \\
&\quad -\frac{1}{2\rho c_{\mathrm{P}}} \sum_{f\in\mathcal{F}_K} \big(\mathbf{n}_K \cdot ([\boldsymbol{\sigma}]_{K,f}\mathbf{n}_K + \rho c_{\mathrm{P}}[\mathbf{v}]_{K,f}), \mathbf{n}_K \cdot (\boldsymbol{\sigma}_{K,h}\mathbf{n}_K + \rho c_{\mathrm{P}}\mathbf{v}_{K,h})\big)_{0,f}\Big) \\
&= \sum_{f\in\mathcal{F}_K} \Big(\frac{1}{\rho c_{\mathrm{S}}}\big\|\mathbf{n}_K \times [\boldsymbol{\sigma}]_{K,f}\mathbf{n}_K\big\|_{0,f}^2 + \rho c_{\mathrm{S}}\big\|\mathbf{n}_K \times [\mathbf{v}_h]_{K,f}\big\|_{0,f}^2 \\
&\qquad\qquad + \frac{1}{\rho c_{\mathrm{P}}}\big\|\mathbf{n}_K \cdot [\boldsymbol{\sigma}]_{K,f}\mathbf{n}_K\big\|_{0,f}^2 + \rho c_{\mathrm{P}}\big\|\mathbf{n}_K \cdot [\mathbf{v}_h]_{K,f}\big\|_{0,f}^2\Big)\,.
\end{aligned}$$

For *acoustic waves* we obtain for $(p_h, \mathbf{v}_h) \in H_h$ and $(\varphi_{K,h}, \boldsymbol{\psi}_{K,h}) \in H_{K,h}$

$$\begin{aligned}\big(A_h(p_h, \mathbf{v}_h), (\varphi_{K,h}, \boldsymbol{\psi}_{K,h})\big)_{0,K} &= -\big(\operatorname{div} \mathbf{v}_{K,h}, \varphi_{K,h}\big)_{0,K} - \big(\nabla p_{K,h}, \boldsymbol{\psi}_{K,h}\big)_{0,K} \\ &\quad - \frac{1}{2\rho c} \sum_{f \in \mathcal{F}_K} \big([p_h]_{K,f} + \rho c \mathbf{n}_K \cdot [\mathbf{v}_h]_{K,f}, \varphi_{K,h} + \rho c \boldsymbol{\psi}_{K,h} \cdot \mathbf{n}_K\big)_{0,f} \,.\end{aligned}$$

On boundary faces $f = \partial K \cap \partial\Omega$, we set $[p_h]_{K,f} = -2p_h$ and $[\mathbf{v}_h]_{K,f} \cdot \mathbf{n}_K = 0$ for Dirichlet boundary conditions, and $[p_h]_{K,f} = 0$ and $[\mathbf{v}_h]_{K,f} \cdot \mathbf{n}_K = -2\mathbf{v}_{K,h} \cdot \mathbf{n}_K$ for Neumann boundary conditions. This yields

$$\big(A_h(p_h, \mathbf{v}_h), (p_h, \mathbf{v}_h)\big)_{0,\Omega} = \frac{1}{2} \sum_{K \in \mathcal{K}} \sum_{f \in \mathcal{F}_K} \Big(\frac{1}{\rho c}\big\|[p_h]_{K,f}\big\|_{0,f}^2 + \rho c \big\|\mathbf{n}_K \cdot [\mathbf{v}_h]_{K,f}\big\|_{0,f}^2\Big).$$

Together with inhomogeneous boundary conditions $p = p_{\mathrm{stat}}$ on Γ_{stat} and $\mathbf{n} \cdot \mathbf{v} = g_{\mathrm{kin}}$ on Γ_{kin} we obtain the semi-discrete equation

$$\begin{aligned}\big(M_h(\partial_t p_h, \partial_t \mathbf{v}_h) + A_h(p_h, \mathbf{v}_h), (\varphi_h, \boldsymbol{\psi}_h)\big)_{0,\Omega} &= \big(\mathbf{b}, \boldsymbol{\psi}_h\big)_{0,\Omega} \\ &\quad + \frac{1}{\rho c} \sum_{f \in \mathcal{F}_K \cap \Gamma_{\mathrm{stat}}} \big(p_{\mathrm{stat}}, \varphi_{K,h} + \rho c \boldsymbol{\psi}_{K,h} \cdot \mathbf{n}_K\big)_{0,f} \\ &\quad + \sum_{f \in \mathcal{F}_K \cap \Gamma_{\mathrm{kin}}} \big(g_{\mathrm{kin}}, \varphi_{K,h} + \rho c \boldsymbol{\psi}_{K,h} \cdot \mathbf{n}_K\big)_{0,f} \,.\end{aligned}$$

4 A Petrov–Galerkin space-time discretization

Let $\overline{Q} = \bigcup_{R\in\mathcal{R}} \overline{R}$ be a decomposition of the space-time cylinder into space-time cells $R = I \times K$ with $K \in \mathcal{K}$ and $I \subset (0,T)$ an interval; $\mathcal{R}$ denotes the set of space-time cells. For every $R \in \mathcal{R}$ we choose local test spaces $W_{h,R} \subset \mathrm{L}_2(R;\mathbb{R}^J)$ and we define the global test space

$$W_h = \Big\{ \mathbf{w}_h \in \mathrm{L}_2((0,T);H) \colon \mathbf{w}_{h,R} = \mathbf{w}_h|_R \in W_{h,R} \Big\}\,.$$

The functions in W_h are discontinuous in space and time. Now we construct $V_h \subset \mathrm{H}^1((0,T);H)$ with $\dim V_h = \dim W_h$. Then, functions in V_h are continuous in time, i.e., $\mathbf{v}_h(\cdot,\mathbf{x})$ is continuous on $[0,T]$ for a.a. $\mathbf{x} \in \Omega$.

In the most simple case this can be achieved for a tensor product space-time discretization with a fixed mesh $\mathcal{K}$ in space and a time series

$$0 = t_0 < t_1 < \cdots < t_N = T\,,$$

i.e., $\mathcal{R} = \big\{ I_n \times K \colon I_n := (t_{n-1},t_n),\ n = 1,\dots,N\,,\ K \in \mathcal{K} \big\}$. Then, we can select a discrete space H_h with $H_{h,K} = \mathbb{P}_p(K;\mathbb{R}^J)$ independently of t, and in every time slice we define $W_{h,R} = H_{h,K}$ constant in time on $R = I_n \times K$. For V_h we use in this case piecewise linear approximations in time

$$\begin{aligned} V_h = \Big\{ &\mathbf{v}_h \in \mathrm{H}^1((0,T);H)\ : \\ &\mathbf{v}_h(0,\mathbf{x}) = \mathbf{0}\,,\ \mathbf{v}_h(t_n,\mathbf{x}) \in H_h \text{ for a.a. } \mathbf{x} \in \Omega \text{ and } n = 1,\dots,N\,, \text{ and} \\ &\mathbf{v}_h(t,\mathbf{x}) = \frac{t_n - t}{t_n - t_{n-1}} \mathbf{v}_h(t_{n-1},\mathbf{x}) + \frac{t - t_{n-1}}{t_n - t_{n-1}} \mathbf{v}_h(t_n,\mathbf{x}) \text{ for } t \in I_n \Big\}\,. \end{aligned}$$

In the more general case, we consider a tensor product space-time mesh with a local selection of polynomial degrees in space and time p_R and q_R in every cell R, and we set for the local test space $W_{h,R} = \mathbb{P}_{q_R-1}(I_n;\mathbb{R}^J) \otimes \mathbb{P}_{p_R}(K;\mathbb{R}^J)$. Then, the local ansatz spaces $V_{h,R} = V_h|_R$ take the form

$$\begin{aligned} V_{h,R} = \Big\{ &\mathbf{v}_{h,R} \in \mathrm{L}_2(R;\mathbb{R}^J)\ : \\ &\mathbf{v}_{h,R}(t,\mathbf{x}) = \frac{t_n - t}{t_n - t_{n-1}} \mathbf{v}_h(t_{n-1},\mathbf{x}) + \frac{t - t_{n-1}}{t_n - t_{n-1}} \mathbf{w}_{h,R}(t,\mathbf{x})\,, \\ &\mathbf{v}_h \in V_h|_{[0,t_{n-1}]}\,,\ \mathbf{w}_{h,R} \in W_{h,R}\,,\ (t,\mathbf{x}) \in R = I_n \times K \Big\}\,. \end{aligned}$$

The discontinuous Galerkin operator in space is extended to the space-time operator $A_h\mathbf{v}_h \in W_h$ by defining for $\mathbf{v}_h \in V_h$ and $\mathbf{w}_h \in W_h$

$$\begin{aligned} \big(A_h\mathbf{v}_h,\mathbf{w}_h\big)_{0,Q} = \sum_{R=I\times K\in\mathcal{R}} \Big(&\big(\operatorname{div}\mathbf{F}(\mathbf{v}_{h,R}),\mathbf{w}_{h,R}\big)_{0,R} \\ &+ \sum_{f\in\mathcal{F}_K} \big(\mathbf{n}_K \cdot (\mathbf{F}_K^{\mathrm{num}}(\mathbf{v}_h) - \mathbf{F}(\mathbf{v}_{h,R})),\mathbf{w}_{h,R}\big)_{0,I\times f} \Big)\,. \end{aligned} \tag{4.1}$$

The discrete space-time operator $L_h \in \mathcal{L}(V_h, W_h)$ and the corresponding discrete bilinear form $b_h(\cdot,\cdot) = \big(L_h\cdot,\cdot\big)_{0,Q}$ are defined by

$$\big(L_h \mathbf{v}_h, \mathbf{w}_h\big)_{0,Q} = \big(M_h \partial_t \mathbf{v}_h + A_h \mathbf{v}_h, \mathbf{w}_h\big)_{0,Q} .$$

In order to show that a solution to our Petrov–Galerkin scheme exists, we check the inf-sup stability of the discrete bilinear form $b_h(\cdot,\cdot)$ with respect to the discrete norm

$$\|\mathbf{v}_h\|_{V_h}^2 = \|\mathbf{v}_h\|_W^2 + \|M_h^{-1} L_h \mathbf{v}_h\|_W^2 . \tag{4.2}$$

By construction, $b_h(\cdot,\cdot)$ is bounded in $V_h \times W_h$, i.e.,

$$\begin{aligned} b_h(\mathbf{v}_h, \mathbf{w}_h) &= \big(L_h \mathbf{v}_h, \mathbf{w}_h\big)_{0,Q} \\ &\le \|M_h^{-1} L_h \mathbf{v}_h\|_W \|\mathbf{w}_h\|_W \le \|\mathbf{v}_h\|_{V_h} \|\mathbf{w}_h\|_W , \qquad \mathbf{v}_h \in V_h ,\ \mathbf{w}_h \in W_h . \end{aligned}$$

For the verification of the inf-sup stability, we introduce the L_2-projection

$$\Pi_h \colon W \to W_h , \qquad \big(\Pi_h \mathbf{v}, \mathbf{w}_h\big)_{0,Q} = \big(\mathbf{v}, \mathbf{w}_h\big)_{0,Q} \qquad \mathbf{w}_h \in W_h .$$

Then, by construction, $\Pi_h A_h = A_h$ and $\Pi_h L_h = L_h$. Moreover, we define the non-negative weight function in time $d_T(t) = T - t$, and we observe

$$\int_0^T \int_0^t \phi(s)\,\mathrm{d}s\mathrm{d}t = \int_0^T d_T(t)\phi(t)\,\mathrm{d}t , \qquad \phi \in L_1(0,T) . \tag{4.3}$$

Lemma 4.1 (Lem. 3 in [8]). *Assume that*

$$\big(M_h \partial_t \mathbf{v}_h, d_T \mathbf{v}_h\big)_{0,Q} \le \big(L_h \mathbf{v}_h, d_T \Pi_h \mathbf{v}_h\big)_{0,Q} , \qquad \mathbf{v}_h \in V_h . \tag{4.4}$$

Then, the bilinear form $b_h(\cdot,\cdot)$ is inf-sup stable in $V_h \times W_h$ with $\beta = 1/\sqrt{1+4T^2}$, i.e.,

$$\sup_{\mathbf{w}_h \in W_h \setminus \{\mathbf{0}\}} \frac{b_h(\mathbf{v}_h, \mathbf{w}_h)}{\|\mathbf{w}_h\|_W} \ge \beta\, \|\mathbf{v}_h\|_{V_h} , \qquad \mathbf{v}_h \in V_h .$$

Referring to [8, Thm. 4.2] we achieve that for given $\mathbf{f} \in L_2(Q;\mathbb{R}^J)$ a unique solution $\mathbf{u}_h \in V_h$ exists solving

$$(L_h \mathbf{u}_h, \mathbf{w}_h)_{0,Q} = (\mathbf{f}, \mathbf{w}_h)_{0,Q} , \qquad \mathbf{w}_h \in W_h \tag{4.5}$$

and satisfying the a priori bound $\|\mathbf{u}_h\|_{V_h} \le \sqrt{4T^2+1}\|M_h^{-1}\Pi_h \mathbf{f}\|_W$.

In the following example we check assumption (4.4) in case of a tensor product discretization with homogeneous polynomial degrees in space and polynomial degree one in time ($q_R \equiv 1$). Note that for this case the Petrov–Galerkin method in time is equivalent to the implicit midpoint rule. A general proof for tensor product discretizations with arbitrary polynomial degrees is given in [8, Lem. 4.4].

Example 4.2. Let $\mathcal{R}$ be a tensor product discretization and $p_R \equiv p$ and $q_R \equiv 1$ for all $R \in \mathcal{R}$. For $\mathbf{v}_h \in V_h$ we set $\mathbf{v}_h^n = \mathbf{v}_h(t_n, \cdot)$. This yields for $t \in I_n = (t_{n-1}, t_n)$

$$\begin{aligned}
\mathbf{v}_h(t, \mathbf{x}) &= \frac{t_n - t}{t_n - t_{n-1}} \mathbf{v}_h^{n-1}(\mathbf{x}) + \frac{t - t_{n-1}}{t_n - t_{n-1}} \mathbf{v}_h^n(\mathbf{x}) \,, \\
\partial_t \mathbf{v}_h(t, \mathbf{x}) &= \frac{1}{t_n - t_{n-1}} \Big(\mathbf{v}_h^n(\mathbf{x}) - \mathbf{v}_h^{n-1}(\mathbf{x}) \Big)
\end{aligned}$$

and thus $\partial_t \mathbf{v}_h = \Pi_h \partial_t \mathbf{v}_h \in W_h$ and $\Pi_h \mathbf{v}_h(\mathbf{x}, t) = \frac{1}{2}(\mathbf{v}_h^{n-1} + \mathbf{v}_h^n)(\mathbf{x})$. Due to

$$\Pi_h \mathbf{v}_h - \mathbf{v}_h = \frac{t_n + t_{n-1} - 2t}{2(t_n - t_{n-1})} \Big(\mathbf{v}_h^n - \mathbf{v}_h^{n-1} \Big)$$

we conclude

$$\begin{aligned}
&\Big(M_h \partial_t \mathbf{v}_h, d_T(\Pi_h \mathbf{v}_h - \mathbf{v}_h) \Big)_{0,Q} \\
&\quad = \sum_{n=1}^{N} \big(M_h(\mathbf{v}_h^n - \mathbf{v}_h^{n-1}), \mathbf{v}_h^n - \mathbf{v}_h^{n-1} \big)_{0,\Omega} \int_{t_{n-1}}^{t_n} d_T(t) \frac{t_n + t_{n-1} - 2t}{2(t_n - t_{n-1})^2} \,\mathrm{d}t \\
&\quad = \sum_{n=1}^{N} \frac{t_n - t_{n-1}}{12} \big(M_h(\mathbf{v}_h^n - \mathbf{v}_h^{n-1}), \mathbf{v}_h^n - \mathbf{v}_h^{n-1} \big)_{0,\Omega} \geq 0
\end{aligned}$$

for all $n = 0, \dots, N$, since $\big(M_h \mathbf{w}_h, \mathbf{w}_h \big)_{0,\Omega} \geq 0$ all $\mathbf{w}_h \in W_h$.
Furthermore, $A_h = \Pi_h A_h$ yields

$$\begin{aligned}
&\big(A_h \mathbf{v}_h, d_T \Pi_h \mathbf{v}_h \big)_{0,Q} \\
&\quad = \big(\Pi_h A_h \mathbf{v}_h, d_T \Pi_h \mathbf{v}_h \big)_{0,Q} \\
&\quad = \sum_{n=1}^{N} \Big(T - \frac{t_{n-1} + t_n}{2} \Big) \frac{t_n - t_{n-1}}{4} \big(A_h(\mathbf{v}_h^{n-1} + \mathbf{v}_h^n), \mathbf{v}_h^{n-1} + \mathbf{v}_h^n \big)_{0,\Omega} \geq 0
\end{aligned}$$

since $T - \frac{1}{2}(t_{n-1} + t_n) \geq 0$ and $\big(A_h \mathbf{v}_h, \mathbf{v}_h \big)_{0,\Omega} \geq 0$ for all $\mathbf{v}_h \in V_h$ by (3.11). Combining both inequalities finally proves assumption (4.4).

Lemma 4.1 directly implies an a priori error estimate in the discrete graph norm (4.2). Let $h = \max_{R \in \mathcal{R}} \operatorname{diam}(R)$ be the mesh size with $\operatorname{diam}(R)^2 = |I|^2 + \operatorname{diam}(K)^2$ for $R = I \times K$. For $1 \leq m \leq \min_R \{p_R + 1, q_R + 1\}$ we have

$$\inf_{\mathbf{v}_h \in V_h \cap \mathrm{H}^1(Q;\mathbb{R}^J)} \|\mathbf{v} - \mathbf{v}_h\|_{1,Q} \leq C h^{m-1} \|\mathbf{v}\|_{m,Q} \,, \qquad \mathbf{v} \in \mathrm{H}^m(Q;\mathbb{R}^J) \tag{4.6}$$

with $C > 0$ depending on the mesh quality.

Theorem 4.3 (Thm. 5 in [8]). *Let* $\mathbf{u} \in V$ *be the solution of* (2.3) *and* $\mathbf{u}_h \in V_h$ *its approximation solving* (4.5). *If the solution satisfies* $\mathbf{u} \in \mathrm{H}^m(Q;\mathbb{R}^J)$ *with* $1 \le m \le \min_R\{p_R+1, q_R+1\}$*, the error can be bounded by*

$$\|\mathbf{u}-\mathbf{u}_h\|_{V_h} \le Ch^{m-1}\,\|\mathbf{u}\|_{m,Q}\,.$$

Proof. Since M_h is the Galerkin projection of M in W, we have

$$b_h(\mathbf{u},\mathbf{w}_h) = b(\mathbf{u},\mathbf{w}_h) = (\mathbf{f},\mathbf{w}_h)_{0,Q} = b_h(\mathbf{u}_h,\mathbf{w}_h)\,, \quad \mathbf{v}_h \in V_h\,,$$

which yields

$$b_h(\mathbf{v}_h-\mathbf{u}_h,\mathbf{w}_h) = b_h(\mathbf{v}_h-\mathbf{u},\mathbf{w}_h) \le \|\mathbf{v}_h-\mathbf{u}\|_{V_h}\|\mathbf{w}_h\|_W\,, \quad \mathbf{v}_h \in V_h\,,$$

and thus

$$\begin{aligned}\|\mathbf{u}-\mathbf{u}_h\|_{V_h} &\le \|\mathbf{u}-\mathbf{v}_h\|_{V_h} + \|\mathbf{v}_h-\mathbf{u}_h\|_{V_h}\\ &\le \|\mathbf{u}-\mathbf{v}_h\|_{V_h} + \beta^{-1}\sup_{\mathbf{w}_h\in W_h\setminus\{\mathbf{0}\}}\frac{b_h(\mathbf{v}_h-\mathbf{u}_h,\mathbf{w}_h)}{\|\mathbf{w}_h\|_W}\\ &\le \big(1+\beta^{-1}\big)\,\|\mathbf{u}-\mathbf{v}_h\|_{V_h}\,.\end{aligned}$$

Now the assertion follows from $\|\mathbf{v}\|_{V_h} \le C\,\|\mathbf{v}\|_{1,Q}$ for $\mathbf{v} \in \mathrm{H}^1(Q;\mathbb{R}^J)$ and (4.6). □

5 Duality based goal-oriented error estimation

In order to develop an adaptive strategy for the selection of the local polynomial degrees p_R, q_R we derive an error indicator with respect to a given linear goal functional $E \in W'$. Following the framework in [4], we define the adjoint problem and solve the dual problem. Then, the error is estimated in terms of the local residual and the dual weight.

The adjoint operator L^* in space and time is defined on the adjoint Hilbert space

$$V^* = \big\{\mathbf{w} \in W\colon \text{there exists } \mathbf{g} \in W \text{ such that } (L\mathbf{v},\mathbf{w})_{0,Q} = (\mathbf{v},\mathbf{g})_{0,Q} \text{ for all } \mathbf{v} \in V\big\}$$

and is characterized by

$$(\mathbf{v}, L^*\mathbf{w})_{0,Q} = (L\mathbf{v},\mathbf{w})_{0,Q}\,, \qquad \mathbf{v} \in V\,,\ \mathbf{w} \in V^*\,.$$

We observe $\big\{\mathbf{v}^* \in \mathrm{C}^1([0,T];\mathcal{D}(A^*))\colon \mathbf{v}^*(T) = \mathbf{0}\big\} \subset V^*$ and $L^* = -L$ on $V \cap V^*$.

For the evaluation of the error functional E we introduce the dual solution $\mathbf{u}^* \in V^*$ defined by

$$(\mathbf{w}, L^*\mathbf{u}^*)_{0,Q} = \langle E,\mathbf{w}\rangle\,, \qquad \mathbf{w} \in W\,.$$

Let $\mathbf{u} \in V$ be the solution of (2.3), and $\mathbf{u}_h \in V_h$ its approximation solving (4.5). Now we derive an exact error representation for the error functional in the case that the dual solution is sufficiently smooth such that $\mathbf{u}^*(t,\cdot)|_f \in \mathrm{L}_2(f;\mathbb{R}^J)$ for all faces $f \in \mathcal{F}_h$ and a.a. $t \in (0,T)$. Inserting the consistency of the numerical flux (3.9) yields for all $\mathbf{w}_h \in W_h \cap V^*$

$$\begin{aligned}
\langle E, \mathbf{u} - \mathbf{u}_h \rangle &= \big(\mathbf{u} - \mathbf{u}_h, -M\partial_t \mathbf{u}^* - \operatorname{div} \mathbf{F}(\mathbf{u}^*)\big)_{0,Q} \\
&= \big(\mathbf{u}, -M\partial_t \mathbf{u}^* - \operatorname{div} \mathbf{F}(\mathbf{u}^*)\big)_{0,Q} - \big(\mathbf{u}_h, -M\partial_t \mathbf{u}^* - \operatorname{div} \mathbf{F}(\mathbf{u}^*)\big)_{0,Q} \\
&= \big(M\partial_t \mathbf{u} + \operatorname{div} \mathbf{F}(\mathbf{u}), \mathbf{u}^*\big)_{0,Q} - \big(\mathbf{u}, \mathbf{n} \cdot \mathbf{F}(\mathbf{u}^*)\big)_{0,\partial Q} \\
&\qquad - \sum_{R \in \mathcal{R}} \Big(\big(M\partial_t \mathbf{u}_h + \operatorname{div} \mathbf{F}(\mathbf{u}_h), \mathbf{u}^*\big)_{0,R} - \big(\mathbf{u}_h, \mathbf{n}_R \cdot \mathbf{F}(\mathbf{u}^*)\big)_{0,\partial R} \Big) \\
&= \big(\mathbf{f}, \mathbf{u}^*\big)_{0,Q} - \sum_{R = I \times K \in \mathcal{R}} \Big(\big(M\partial_t \mathbf{u}_{h,R} + \operatorname{div} \mathbf{F}(\mathbf{u}_{h,R}), \mathbf{u}^*\big)_{0,R} \\
&\qquad\qquad - \big(\mathbf{u}_h, \mathbf{n}_K \cdot \mathbf{F}(\mathbf{u}^*)\big)_{0,I \times \partial K} \Big) \\
&= \sum_{R = I \times K \in \mathcal{R}} \Big(\big(\mathbf{f} - M\partial_t \mathbf{u}_{h,R} - \operatorname{div} \mathbf{F}(\mathbf{u}_{h,R}), \mathbf{u}^*\big)_{0,R} \\
&\qquad\qquad + \big(\mathbf{n}_K \cdot \mathbf{F}(\mathbf{u}_{h,R}), \mathbf{u}^*\big)_{0,I \times \partial K} \Big) \\
&= \sum_{R = I \times K \in \mathcal{R}} \Big(\big(\mathbf{f} - M\partial_t \mathbf{u}_{h,R} - \operatorname{div} \mathbf{F}(\mathbf{u}_{h,R}), \mathbf{u}^* - \mathbf{w}_h\big)_{0,R} \\
&\qquad\qquad + \big(\mathbf{n}_K \cdot \mathbf{F}(\mathbf{u}_{h,R}), \mathbf{u}^* - \mathbf{w}_h\big)_{0,I \times \partial K} \Big) .
\end{aligned}$$

However, this identity cannot be evaluated numerically since it depends on the unknown function $\mathbf{u}^*$. In applications, the following heuristic error bound is used instead. Let $\mathbf{u}_h^* \in W_h$ be a numerical approximation of the dual solution given by

$$b_h(\mathbf{v}_h, \mathbf{u}_h^*) = \langle E, \mathbf{v}_h \rangle , \qquad \mathbf{v}_h \in V_h .$$

Inserting some interpolation $\mathbf{w}_h = I_h \mathbf{u}^*$, the interpolation error $\mathbf{u}^* - I_h \mathbf{u}^*$ has to be estimated in terms of $\mathbf{u}_h^*$. For this purpose we use also the face jumps $[\mathbf{u}_h^*]_{K,f}$ which are also meaningful in case of piecewise constant approximations in W_h. In case of higher order approximations in W_h we use $[Q_h \mathbf{u}_h^*]_{K,f}$, where Q_h denotes the piecewise L_2-projection in space to $\mathbb{P}_0(K;\mathbb{R}^J)$.

Finally, $|\langle E, \mathbf{u} - \mathbf{u}_h \rangle|$ is estimated by $\sum_{R \in \mathcal{R}} \eta_R$ with local contributions η_R depending on residual terms and jump terms of the discrete solution and on jump terms of the dual approximation.

For elastic waves we obtain for $(\boldsymbol{\varphi}_h, \boldsymbol{\psi}_h) \in W_h \cap V^*$ the error representation

$$\begin{aligned}
\big\langle E, (\boldsymbol{\sigma} - \boldsymbol{\sigma}_h, \mathbf{v} - \mathbf{v}_h)\big\rangle = \sum_{R = I \times K \in \mathcal{R}} \Big(& \big(- \mathbf{C}^{-1}\partial_t \boldsymbol{\sigma}_{h,R} + \boldsymbol{\varepsilon}(\mathbf{v}_{h,R}), \boldsymbol{\sigma}^* - \boldsymbol{\varphi}_h\big)_{0,R} \\
& + \big(\mathbf{b} - \rho \partial_t \mathbf{v}_{h,R} + \operatorname{div} \boldsymbol{\sigma}_{h,R}, \mathbf{v}^* - \boldsymbol{\psi}_h\big)_{0,R} \\
& + \big(\mathbf{v}_{h,R}, (\boldsymbol{\sigma}^* - \boldsymbol{\varphi}_h)\mathbf{n}_K\big)_{0,I\times\partial K} \\
& + \big(\boldsymbol{\sigma}_{R,h}\mathbf{n}_K, \mathbf{v}^* - \boldsymbol{\psi}_h\big)_{0,I\times\partial K}\Big) \\
= \sum_{R = I \times K \in \mathcal{R}} \Big(& \big(- \mathbf{C}^{-1}\partial_t \boldsymbol{\sigma}_{h,R} + \boldsymbol{\varepsilon}(\mathbf{v}_{h,R}), \boldsymbol{\sigma}^* - \boldsymbol{\varphi}_h\big)_{0,R} \\
& + \big(\mathbf{b} - \rho \partial_t \mathbf{v}_{h,R} + \operatorname{div} \boldsymbol{\sigma}_{h,R}, \mathbf{v}^* - \boldsymbol{\psi}_h\big)_{0,R} \\
& + \frac{1}{2}\sum_{f \in \mathcal{F}_K} \Big(\big([\mathbf{v}_h]_{K,f}, (\boldsymbol{\sigma}^* - \boldsymbol{\varphi}_h)\mathbf{n}_K\big)_{0,I\times f} \\
& \qquad + \big([\boldsymbol{\sigma}_h]_{K,f}\mathbf{n}_K, \mathbf{v}^* - \boldsymbol{\psi}_h\big)_{0,I\times f}\Big)\Big) .
\end{aligned}$$

This motivates the local error estimate

$$\begin{aligned}
\eta_R = & \big\| - \mathbf{C}^{-1}\partial_t \boldsymbol{\sigma}_{h,R} + \boldsymbol{\varepsilon}(\mathbf{v}_{h,R})\big\|_{0,R} h_K^{1/2} \big\|[Q_h \boldsymbol{\sigma}_h^*]_K \mathbf{n}_K\big\|_{0,I\times\partial K} \\
& + \big\|\mathbf{b} - \rho\partial_t \mathbf{v}_{h,R} + \operatorname{div}\boldsymbol{\sigma}_{h,R}\big\|_{0,R} h_K^{1/2}\big\|[Q_h \mathbf{v}_h^*]_K\big\|_{0,I\times\partial K} \\
& + \frac{1}{2}\sum_{f\in\mathcal{F}_K}\Big(\big\|[\mathbf{v}_h]_{K,f}\|_{0,I\times f}\big\|[Q_h\boldsymbol{\sigma}_h^*]_{K,f}\mathbf{n}_K\big\|_{0,I\times f} \\
& \qquad + \big\|[\boldsymbol{\sigma}_h]_{K,f}\mathbf{n}_K\|_{0,I\times f}\big\|[Q_h\mathbf{v}_h^*]_{K,f}\big\|_{0,I\times f}\Big) ,
\end{aligned}$$

where the jump terms $[Q_h\boldsymbol{\sigma}_h^*]_{K,f}$ and $[Q_h\mathbf{v}_h^*]_{K,f}$ are used to estimate the best approximation error of $(\boldsymbol{\sigma}^* - \boldsymbol{\varphi}_h)\mathbf{n}_K$ and $\mathbf{v}^* - \boldsymbol{\psi}_h$.

In the same way we obtain for acoustic waves the error representation

$$\begin{aligned}
\big\langle E, (p - p_h, \mathbf{v} - \mathbf{v}_h)\big\rangle = \sum_{R = I \times K \in \mathcal{R}} \Big[& \big(- \kappa^{-1}\partial_t p_{h,R} + \operatorname{div}\mathbf{v}_{h,R}, p^* - \varphi_h\big)_{0,R} \\
& + \big(\mathbf{b} - \rho\partial_t \mathbf{v}_{h,R} + \nabla p_{h,R}, \mathbf{v}^* - \boldsymbol{\psi}_h\big)_{0,R} \\
& + \frac{1}{2}\sum_{f\in\mathcal{F}_K}\Big(\big(\mathbf{n}_K\cdot[\mathbf{v}_h]_{K,f}, p^* - \varphi_h\big)_{0,I\times f} \\
& \qquad + \big([p_h]_{K,f}, \mathbf{n}_K\cdot(\mathbf{v}^* - \boldsymbol{\psi}_h)\big)_{0,I\times f}\Big)\Big]
\end{aligned}$$

and the local error estimate

$$\begin{aligned}
\eta_R = \big\| -\kappa^{-1}\partial_t p_{h,R} + \operatorname{div} \mathbf{v}_{h,R}\big\|_{0,R} h_K^{1/2} \big\|[Q_h p_h^*]_K\big\|_{0,I\times\partial K} \\
+ \big\|\mathbf{b} - \rho\partial_t \mathbf{v}_{h,R} + \nabla p_{h,R}\big\|_{0,R} h_K^{1/2} \big\|\mathbf{n}_K \cdot [Q_h \mathbf{v}_h^*]_K\big\|_{0,I\times\partial K} \\
+ \frac{1}{2}\sum_{f\in\mathcal{F}_K} \Big(\big\|[\mathbf{v}_h]_{K,f}\|_{0,I\times f} \big\|[Q_h p_h^*]_{K,f}\big\|_{0,I\times f} \\
+ \big\|[p_h]_{K,f}\mathbf{n}_K\|_{0,I\times f} \big\|\mathbf{n}_K \cdot [Q_h \mathbf{v}_h^*]_{K,f}\big\|_{0,I\times f}\Big)\,.
\end{aligned}$$

In our examples we use the adaptive strategy for p-refinement described in Algorithm 1. It depends on a parameter $\vartheta < 1$ for the adaptive selection criterion.

Algorithm 1 Adaptive algorithm.

```
choose low order polynomial degrees on the initial mesh
while max_R(p_R) < p_max and max_R(q_R) < q_max do
    compute u_h
    compute u*_h and the projection Q_h u*_h
    compute η_R on every cell R
    if the error is small enough STOP
    mark space-time cell R if η_R > ϑ max_R' η_R'
    increase polynomial degrees on marked cells by one
    redistribute cells on processes for better load balancing
end while
```

6 Space-time multilevel preconditioner

In this section we address the numerical aspects and in particular solution methods for the discrete hyperbolic space-time problem. First we describe the realization of our discretization using nodal basis functions in space and time, and then a multilevel preconditioner is introduced.

Nodal Discretization Now we consider the structure of the linear system for the special case of a tensor product space-time mesh $\mathcal{R} = \bigcup_{n=1}^N \mathcal{R}^n$ with time slices $\mathcal{R}^n = \big\{I_n \times K \colon K \in \mathcal{K}\big\}$ and variable polynomial degrees p_R, q_R in every space-time cell R, cf. Sect. 4. Let $\{\boldsymbol{\psi}^n_{R,j}\}_{j=1,\dots,\dim W_{h,R}}$ be a basis of $W_{h,R}$ and define $W_h^n = \operatorname{span}\Big\{\bigcup_{R\in\mathcal{R}^n}\bigcup_{j=1}^{\dim W_{h,R}} \boldsymbol{\psi}^n_{R,j}\Big\}$. Then, the solution $\mathbf{u}_h \in V_h$ is represented by finite element functions $\mathbf{u}_h^n \in W_h^n$, $n = 1,\dots,N$. Together with $\mathbf{u}_h^0 = \mathbf{0}$ we obtain

$$\mathbf{u}_h(t,\mathbf{x}) = \frac{t_n - t}{t_n - t_{n-1}}\mathbf{u}_h^{n-1}(t_{n-1},\mathbf{x}) + \frac{t - t_{n-1}}{t_n - t_{n-1}}\mathbf{u}_h^n(t,\mathbf{x})\,, \qquad (t,\mathbf{x}) \in I_n \times K\,.$$

The corresponding coefficient vector of the solution is denoted by $\underline{u} = (\underline{u}^1, \dots, \underline{u}^N)^\top$, where $\underline{u}^n \in \mathbb{R}^{\dim W_h^n}$ is the coefficient vector of $\mathbf{u}_h^n = \sum_{R\in\mathcal{R}^n} \sum_{j=1}^{\dim W_{h,R}} \underline{u}_{R,j}^n \boldsymbol{\psi}_{R,j}^n$. With respect to this basis, the discrete space-time system (4.5) has the matrix representation $\underline{L}\,\underline{u} = \underline{f}$ with the block matrix

$$\underline{L} = \begin{pmatrix} \underline{D}^1 & & & \\ \underline{C}^1 & \underline{D}^2 & & \\ & \ddots & \ddots & \\ & & \underline{C}^{N-1} & \underline{D}^N \end{pmatrix}$$

and matrix entries

$$\underline{D}^n_{R',k,R,j} = \int_{t_{n-1}}^{t_n} \int_\Omega L_h\Big(\frac{t-t_{n-1}}{t_n - t_{n-1}} \boldsymbol{\psi}^n_{R,j}(t,\mathbf{x})\Big) \boldsymbol{\psi}^n_{R',k}(t,\mathbf{x})\,\mathrm{d}\mathbf{x}\mathrm{d}t\,, \qquad R,R' \in \mathcal{R}^n$$

$$\underline{C}^n_{R',k,R,j} = \int_{t_{n-1}}^{t_n} \int_\Omega L_h\Big(\frac{t_n - t}{t_n - t_{n-1}} \boldsymbol{\psi}^{n-1}_{R,j}(t_{n-1},\mathbf{x})\Big) \boldsymbol{\psi}^n_{R',k}(t,\mathbf{x})\,\mathrm{d}\mathbf{x}\mathrm{d}t\,,$$
$$R \in \mathcal{R}^{n-1}\,,\ R' \in \mathcal{R}^n\,,$$

and the right-hand side $\underline{f} = (\underline{f}^1, \dots, \underline{f}^N)$ with $\underline{f}^n_{j,R} = (\mathbf{f}, \boldsymbol{\psi}^n_{R,j})_{0,R}$. Sequentially, this system can be solved by a block-Gauss–Seidel method (corresponding to implicit time integration)

$$\underline{D}^1\underline{u}^1 = \underline{f}^1\,, \quad \underline{D}^2\underline{u}^2 = \underline{f}^2 - \underline{C}^1\underline{u}^1\,, \quad \dots, \quad \underline{D}^N\underline{u}^N = \underline{f}^N - \underline{C}^{N-1}\underline{u}^{N-1}\,,$$

provided that $\underline{D}^n$ can be inverted efficiently.

Multilevel methods For space-time multilevel preconditioners we consider hierarchies in space and time. Therefore, let $\mathcal{R}_{0,0}$ be the coarse space-time mesh, and let $\mathcal{R}_{l,k}$ be the discretization obtained by $l = 1, \dots, l_{\max}$ uniform refinements in space and $k = 1, \dots, k_{\max}$ refinements in time. Let $V_{l,k}$ be the approximation spaces on $\mathcal{R}_{l,k}$ with fixed polynomial degrees $p_R \equiv p$ and $q_R \equiv q$. Let $\underline{L}_{l,k}$ be the corresponding matrix representation of the discrete operator L_h in $V_{l,k}$.

The multilevel preconditioner combines smoothing operations on different levels and requires transfer matrices between the levels. Since the spaces are nested, we can define prolongation matrices $\underline{P}^{l,k}_{l-1,k}$ and $\underline{P}^{l,k}_{l,k-1}$ representing the natural injections $V_{l-1,k} \subset V_{l,k}$ in space and $V_{l,k-1} \subset V_{l,k}$ in time. Correspondingly, the restriction matrices $\underline{R}^{l,k}_{l-1,k}$ and $\underline{R}^{l,k}_{l,k-1}$ represent the L_2-projections in space and in time of the test spaces $W_{l,k} \supset W_{l-1,k}$ and $W_{l,k} \supset W_{l,k-1}$.

For the smoothing operations on level (l,k) we consider the block-Jacobi preconditioner or the block-Gauss–Seidel preconditioner (where all components corresponding to a space-time cell R build a block)

$$\underline{B}^{\mathrm{J}}_{l,k} = \theta_{l,k}\,\text{block\_diag}(\underline{L}_{l,k})^{-1}\,,$$
$$\underline{B}^{\mathrm{GS}}_{l,k} = \theta_{l,k}\,\big(\text{block\_lower}(\underline{L}_{l,k}) + \text{block\_diag}(\underline{L}_{l,k})\big)^{-1}$$

with damping parameter $\theta_{l,k} \in (0,1]$. The corresponding iteration matrices are given by $\underline{S}^{\mathrm{J}}_{l,k} = \underline{\mathrm{Id}}_{l,k} - \underline{B}^{\mathrm{J}}_{l,k}\underline{L}_{l,k}$ and $\underline{S}^{\mathrm{GS}}_{l,k} = \underline{\mathrm{Id}}_{l,k} - \underline{B}^{\mathrm{GS}}_{l,k}\underline{L}_{l,k}$, and the number of pre- and post-smoothing steps are denoted by $\nu^{\mathrm{pre}}_{l,k}$ and $\nu^{\mathrm{post}}_{l,k}$.

Now, the multilevel preconditioner $\underline{B}^{\mathrm{ML}}_{l,k}$ is defined recursively. On the coarse level, we use a parallel direct linear solver $\underline{B}^{\mathrm{ML}}_{0,0} = \big(\underline{L}_{0,0}\big)^{-1}$, see [26, 27]. Then, we have two options: restricting in time defines $\underline{B}^{\mathrm{ML}}_{l,k}$ by

$$\begin{aligned}&\underline{\mathrm{Id}}_{l,k} - \underline{B}^{\mathrm{ML}}_{l,k}\underline{L}_{l,k}\\ &\quad= \Big(\underline{\mathrm{Id}}_{l,k} - \underline{B}^{\mathrm{J}}_{l,k}\underline{L}_{l,k}\Big)^{\nu^{\mathrm{pre}}_{l,k}}\Big(\underline{\mathrm{Id}}_{l,k} - \underline{P}^{l,k}_{l,k-1}\underline{B}^{\mathrm{ML}}_{l,k-1}\underline{R}^{l,k}_{l,k-1}\underline{L}_{l,k}\Big)\Big(\underline{\mathrm{Id}}_{l,k} - \underline{B}^{\mathrm{J}}_{l,k}\underline{L}_{l,k}\Big)^{\nu^{\mathrm{post}}_{l,k}}\end{aligned}$$

with Jacobi smoothing, and restricting in space yields

$$\begin{aligned}&\underline{\mathrm{Id}}_{l,k} - \underline{B}^{\mathrm{ML}}_{l,k}\underline{L}_{l,k}\\ &\quad= \Big(\underline{\mathrm{Id}}_{l,k} - \underline{B}^{\mathrm{GS}}_{l,k}\underline{L}_{l,k}\Big)^{\nu^{\mathrm{pre}}_{l,k}}\Big(\underline{\mathrm{Id}}_{l,k} - \underline{P}^{l,k}_{l-1,k}\underline{B}^{\mathrm{ML}}_{l-1,k}\underline{R}^{l,k}_{l-1,k}\underline{L}_{l,k}\Big)\Big(\underline{\mathrm{Id}}_{l,k} - \underline{B}^{\mathrm{GS}}_{l,k}\underline{L}_{l,k}\Big)^{\nu^{\mathrm{post}}_{l,k}}\end{aligned}$$

with Gauss–Seidel smoothing. Our tests in [8] indicate that it is advantegeous to start with refinement in time and then refinement in space, i.e, we use the sequence of meshes $\mathcal{R}_{0,0}, \mathcal{R}_{0,1}, \dots, \mathcal{R}_{0,k_{\max}}, \mathcal{R}_{1,k_{\max}}, \dots, \mathcal{R}_{l_{\max},k_{\max}}$ (see Algorithm 2 for the recursive realization of the multilevel preconditioner).

Algorithm 2 Multilevel preconditioner $\underline{c}_{l,k} = \underline{B}^{\mathrm{ML}}_{l,k}\underline{r}_{l,k}$ with Gauss–Seidel smoother $\underline{B}^{\mathrm{SM}}_{l,k} = \underline{B}^{\mathrm{GS}}_{l,k}$ in space for $l > 0$ or Jacobi smoother $\underline{B}^{\mathrm{SM}}_{0,k} = \underline{B}^{\mathrm{J}}_{0,k}$ in time

$\underline{c}_{l,k} = \underline{0}$
for $\nu = 1, \dots, \nu^{\mathrm{pre}}_{lk}$ **do**
  $\underline{w}_{l,k} = \underline{B}^{\mathrm{SM}}_{l,k}\underline{r}_{l,k}$
  $\underline{c}_{l,k} := \underline{c}_{l,k} + \underline{w}_{l,k}$ and $\underline{r}_{l,k} := \underline{r}_{l,k} - \underline{L}_{l,k}\underline{w}_{l,k}$
end for
$\underline{r}_{l-1,k} = \underline{R}^{l,k}_{l-1,k}\underline{r}_{l,k}$ for $l > 0$ or $\underline{r}_{0,k-1} = \underline{R}^{l,k}_{0,k-1}\underline{r}_{0,k}$
$\underline{c}_{l-1,k} = \underline{B}^{\mathrm{ML}}_{l-1,k}\underline{r}_{l-1,k}$ for $l > 0$ or $\underline{c}_{0,k-1} = \underline{B}^{\mathrm{ML}}_{0,k-1}\underline{r}_{0,k-1}$
$\underline{w}_{l,k} = \underline{P}^{l,k}_{l-1,k}\underline{c}_{l-1,k}$ for $l > 0$ or $\underline{w}_{0,k} = \underline{P}^{l,k}_{0,k-1}\underline{c}_{0,k-1}$
$\underline{c}_{l,k} := \underline{c}_{l,k} + \underline{w}_{l,k}$ and $\underline{r}_{l,k} := \underline{r}_{l,k} - \underline{L}_{l,k}\underline{w}_{l,k}$
for $\nu = 1, \dots, \nu^{\mathrm{post}}_{lk}$ **do**
  $\underline{w}_{l,k} = \underline{B}^{\mathrm{SM}}_{l,k}\underline{r}_{l,k}$
  $\underline{c}_{l,k} := \underline{c}_{l,k} + \underline{w}_{l,k}$ and $\underline{r}_{l,k} := \underline{r}_{l,k} - \underline{L}_{l,k}\underline{w}_{l,k}$
end for

7 Numerical experiments

We illustrate the numerical performance of the space-time method with two examples. The first test is a simple plane wave solution for the acoustic problem where the solution is known so that we can test the convergence properties for uniform h- and p-refinement. The second example is application-oriented and shows the behavior of the p-adaptive algorithm for a configuration motivated from tunnel exploration.

In all cases the linear systems are solved approximately with a GMRES iteration and the space-time multigrid preconditioner. As general multigrid parameters we use for coarsening in time a damped block-Jacobi preconditioner ($\theta = 0.5$) with 2 pre- and post-smoothing steps, and for coarsening in space a block-Gauss–Seidel preconditioner with 5 pre- and post-smoothing steps. A V-cycle with coarsening the mesh first in space and then in time is applied. All computations use multigrid over three levels in space and in time.

The adaptive refinement starts with a finite volume discretization in space ($p = 0$), and linear ansatz and constant test functions in time on each space-time cell ($q = 1$). The algorithm increases in the first step adaptively the polynomial degrees in space and later the polynomial degrees in space and time simultaneously. The approximation spaces $V_{l,k}$ are chosen such that the polynomial degrees on each cell is the maximum over all corresponding cells of the fine mesh. For the underlying 2D mesh in space we use quadrilaterals.

7.1 A benchmark experiment

The first example is specially designed for a convergence test. We use the time interval $(0,T) = (0,4)$ and the spatial domain $\Omega = (-2,4) \times (0,2) \subset \mathbb{R}^2$ with piecewise constant parameters

$$\rho(x_1,x_2) = \begin{cases} 1 & x_1 < 0, \\ 2 & 0 < x_1 < 1, \\ 1/2 & 1 < x_1\,, \end{cases} \qquad \text{and} \qquad \kappa(\mathbf{x}) = 1/\rho(\mathbf{x})\,.$$

Starting with

$$\mathbf{u}_0(\mathbf{x}) = A(x_1)\begin{pmatrix}1\\1\\0\end{pmatrix} \text{ for } A(x_1) = \begin{cases} \cos((x_1-1)\pi/2)^6 & -2 < x_1 < 0\,, \\ 0 & \text{else} \end{cases}$$

results in the plane wave solution with

$$\mathbf{u}(t,x_1,x_2) = \begin{cases} \mathbf{u}_0(x_1 - t, x_2) & x_1 \le 0\,, \\ \mathbf{u}_0(2x_1 - t, x_2) & 0 < x_1 \le 1\,, \\ \mathbf{u}_0(2 + 0.5(x_1-1) - t, x_2) & 1 \le x_1\,. \end{cases}$$

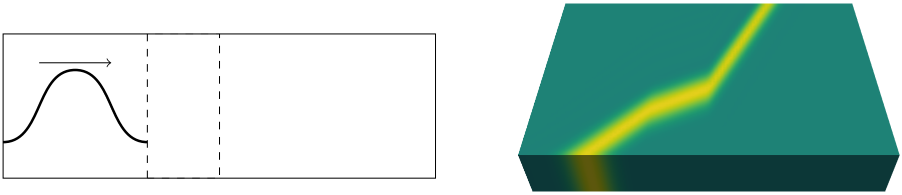

Figure 1. Benchmark experiment: The initial wave will travel from the left to the right. Sketch of the impulse (left) and pressure component of the space-time solution (right).

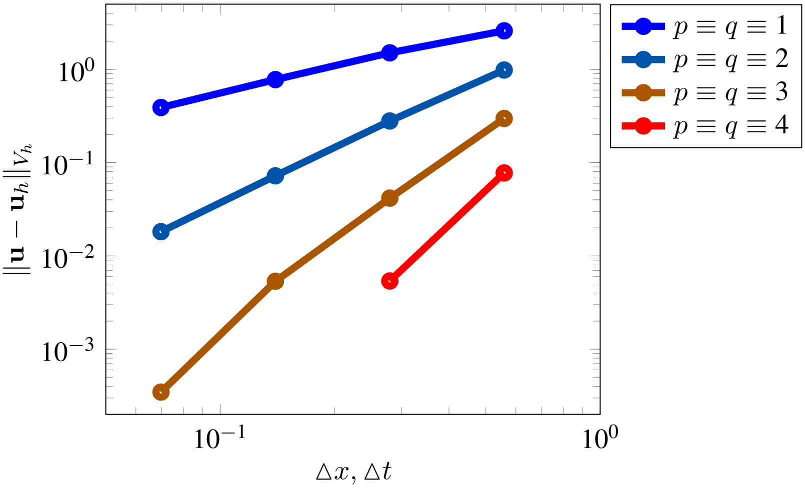

	$p=q=1$		$p=q=2$		$p=q=3$		$p=q=4$	
st-cells	st-DoF	$\|\mathbf{e}_h\|_{V_h}$	st-DoF	$\|\mathbf{e}_h\|_{V_h}$	st-DoF	$\|\mathbf{e}_h\|_{V_h}$	st-DoF	$\|\mathbf{e}_h\|_{V_h}$
1 536	18 432	2.5916	82 944	0.9841	221 184	0.2974	460 800	0.0775
12 288	147 456	1.5041	663 552	0.2796	1 769 472	0.0416	3 686 400	0.0054
98 304	1 179 648	0.7772	5 308 416	0.0722	14 155 776	0.0053	29 491 200	3.468-4
786 432	9 437 184	0.3900	42 467 328	0.0182	out of memory		out of memory	
EOC		0.995		1.989		2.961		3.960

Table 3. Benchmark experiment: Convergence of the error $\mathbf{e}_h = \mathbf{u} - \mathbf{u}_h$ with respect to the norm $\|\cdot\|_{V_h}$ and extrapolated orders of convergence (EOC) for uniformly refined space-time meshes and different polynomial degrees.

The computed experimental orders of convergence are shown in Table 3. We observe the expected order of convergence as predicted in Theorem 4.3 for sufficiently smooth solutions.

7.2 A tunnel experiment

The second example illustrates seismic tunnel exploration: An artificially generated surface wave in the tunnel propagates into the solid and the reflected waves are measured in a certain region. Here, we compare the results of acoustic and elastic waves.

We choose a rectangular domain $\Omega \subset (-2,2) \times (-1.5,2.5) \subset \mathbb{R}^2$ and we use density $\rho = 1$, Lamé parameters $\lambda = 0.5$ and $\mu = 0.25$ for the elastic wave equation. This results in compression waves with velocity $c_{\mathrm{P}} = \sqrt{(2\mu+\lambda)/\rho} = 1$ and shear waves with velocity $c_{\mathrm{S}} = \sqrt{\mu/\rho} = 0.5$. In the acoustic case we use the parameters $\rho = \kappa = 1$, so that the velocity of sound $c = \sqrt{\kappa/\rho} = 1$ is equal to the wave propagation speed of the elastic compression waves.

At $t = 0$ we start with a smooth pulse located at $\mathbf{x}_{\mathrm{mid}} = (0.5, 1) \in \partial\Omega$ defining the initial velocity

$$\mathbf{v}_0 = \begin{pmatrix} x_1 - 0.5 \\ x_2 - 1.0 \end{pmatrix} \phi \quad \text{with} \quad \phi(\mathbf{x}) = \begin{cases} \cos^6\left(2\pi|\mathbf{x}_{\mathrm{mid}} - \mathbf{x}|^2\right) & |\mathbf{x}_{\mathrm{mid}} - \mathbf{x}|^2 < 0.25\,, \\ 0 & \text{else.} \end{cases}$$

In the acoustic case we set $p_0 \equiv 0$ and in the elastic case $\boldsymbol{\sigma}_0 \equiv \mathbf{0}$.

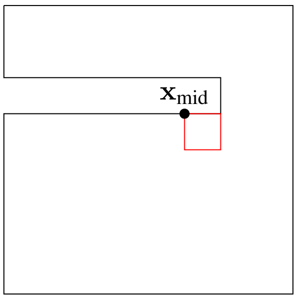

Figure 2. Tunnel experiment: Sketch of the computional domain Ω with marked region of interest RoI.

In applications the velocity is measured at certain points within a region of interest RoI; here we use $\mathrm{RoI} = (0.5,1) \times (0.5,1)$, cf. Figure 2. Since we are interested in the velocity at the final time $T = 3$, we consider the linear goal functional

$$E(\mathbf{v}) = \frac{1}{|\mathrm{RoI}|} \int\limits_{\mathrm{RoI}\times\{T\}} v_1 \,\mathrm{d}\mathbf{x}\,.$$

The smooth pulse starts at $\mathbf{x}_{\mathrm{mid}}$ and expands through the domain. After being reflected at the right boundary, the wave reaches back to the region of interest. The visualization is obtained by slicing through the space-time mesh, see Figure 3.

Figure 3. Acoustic wave: Slices through the space-time mesh of the pressure component.

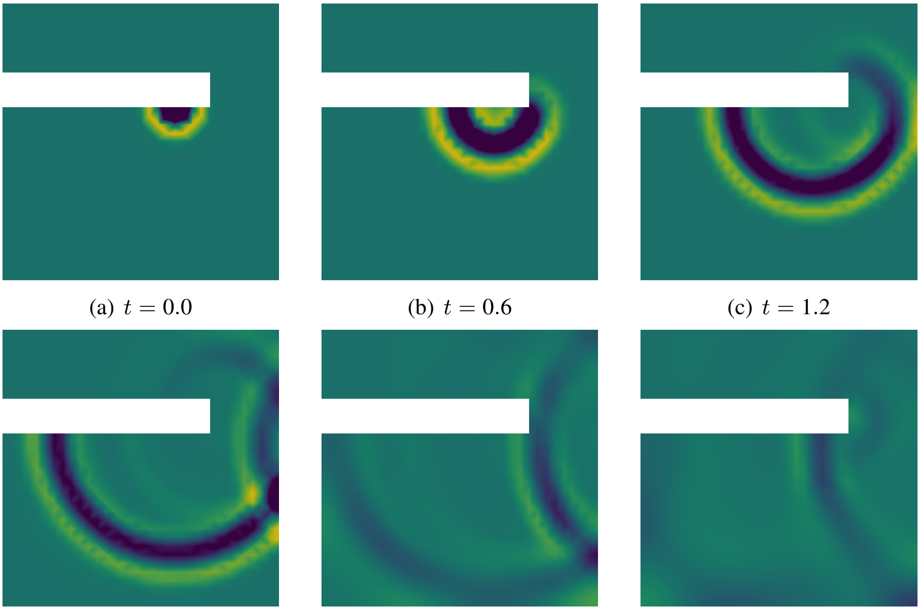

(a) $t = 0.0$ (b) $t = 0.6$ (c) $t = 1.2$

(d) $t = 1.8$ (e) $t = 2.4$ (f) $t = 3.0$

ref-step	(p, q)	#DoF (effort)	GMRES steps with MG-PC	$E(\mathbf{u_h})$	$\triangle E_{\text{ex}}(\mathbf{u_h})$
		uniform refinement			
$r = 1$	$(1, 1)$	534 528	7	4.9961e-3	9.09e-5
$r = 2$	$(2, 2)$	2 405 376	13	4.8946e-3	1.06e-5
$r = 3$	$(3, 3)$	6 414 336	19	4.8810e-3	2.42e-5
$r = 4$	$(4, 4)$	13 363 200	27	4.8931e-3	1.21e-5
		adaptive refinement			
$r = 0$	$(0, 1)$	133 632	5	4.4104e-4	4.46e-3
$r = 1$		291 411 (55%)	7	4.9677e-3	6.25e-5
$r = 2$		819 279 (34%)	13	4.8767e-3	2.85e-5
$r = 3$		1 875 753 (29%)	20	4.8779e-3	2.73e-5
$r = 4$		3 594 969 (27%)	28	4.8866e-3	1.86e-5

Table 4. Acoustic wave: Uniform vs. adaptive refinement on $44\,544 = 928 \times 48$ space-time cells distributed on 64 processor cores. The error $\triangle E_{\text{ex}}(\mathbf{u_h}) = |E(\mathbf{u_h}) - E_{\text{ex}}|$ of the goal functional is approximately estimated with respect to a linear extrapolation of the uniform results $E_{\text{ex}} = 4.9052\text{e-}3$.

The results for the uniform and adaptive refinement in the acoustic case are given in Table 4. We observe that the adaptive algorithm saves over 70% of the degrees of freedom while achieving the same accuracy compared with uniform refinement.

ref-step	(p, q)	#DoF (effort)	GMRES steps with MG-PC	$E(\mathbf{u_h})$	$\triangle E_{\text{ex}}$
		uniform refinement			
$r = 1$	$(1, 1)$	890 880	5	1.3625e-3	5.43e-4
$r = 2$	$(2, 2)$	4 008 960	7	1.7686e-3	1.37e-4
$r = 3$	$(3, 3)$	10 690 560	8	1.8371e-3	6.86e-5
		adaptive refinement			
$r = 0$	$(0, 1)$	222 720	5	4.7218e-4	1.43e-3
$r = 1$		551 370 (62%)	6	1.1362e-3	5.44e-4
$r = 2$		1 477 655 (37%)	7	1.7687e-3	1.37e-4
$r = 3$		3 379 390 (32%)	9	1.8371e-3	6.86e-5
$r = 4$		6 510 765 (29%)	11	1.8723e-3	3.34e-5

Table 5. Elastic wave: Uniform vs. adaptive refinement on $44\,544 = 928 \times 48$ space-time cells distributed to 64 processor cores (for uniform computations $p = q \leq 3$ due to memory restrictions). The error of the goal functional is approximately estimated with respect to $E_{\text{ex}} = 1.9057\text{e-}3$.

Comparing the acoustic wave in Figure 3 with the results in Figure 5 for the elastic wave we can see the additional shear wave which propagates with half of the velocity behind the compression wave. The acoustic wave equation in 2D has three components and the elastic wave equation has five components. This results in more DoF and thus in larger matrices. To save random access memory in this case we use as approximation spaces $V_{l,k}$ on the coarser meshes a lowest order finite volume discretization. The results for uniform and adaptive refinement in the elastic case are shown in Table 5 and illustrated in Figure 5, which demonstrates the excellent efficiency of the adaptive scheme.

Figure 4. Tunnel Experiment: Strong scaling for ~ 34 Mio. DoFs (acoustic wave).

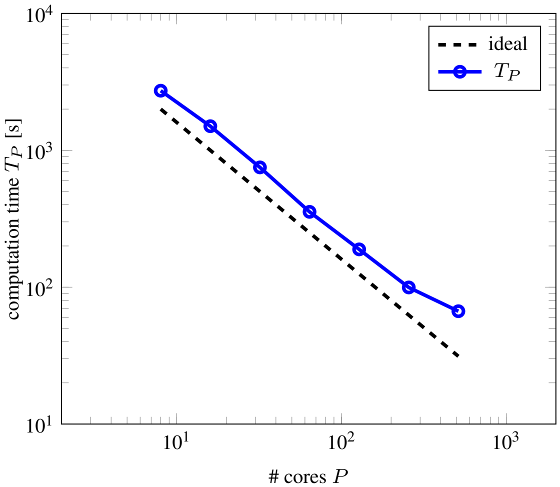

The parallel scaling behavior of the parallel multilevel preconditioner is tested for different numbers of processes. On mesh level 4 we have 2 850 816 space-time cells, a linear discretization in space and time results in 34 209 792 DoFs for the acoustic case. The computing time for solving this huge linear system system with the parallel multigrid method scales nearly optimal[1], cf. Figure 4.

Bibliography

[1] R. Andreev and C. Tobler, Multilevel preconditioning and low-rank tensor iteration for space-time simultaneous discretizations of parabolic PDEs, *Numer. Linear Algebra Appl.* 22 (2015), 317–337.

[2] U. M. Ascher, S. J. Ruuth and B. T. R., Implicit-explicit methods for time-dependent partial differential equations, *SIAM J. Numer. Anal.* 32 (1995), 797–823.

[3] W. Bangerth and R. Rannacher, Finite element approximation of the acoustic wave equation: error control and mesh adaptation, *East-West J. Numer. Math.* 7 (1999), 263–282.

[4] ______, *Adaptive finite element methods for differential equations*, Birkhäuser Verlag, Basel, 2003.

[5] C. Cong, X.-C. Cai and K. Gustafson, Implicit space-time domain decomposition methods for stochastic parabolic partial differential equations, *SIAM J. Sci. Comput.* 36 (2014), C1–C24.

[6] L. F. Demkowicz and J. Gopalakrishnan, *An overview of the discontinuous Petrov–Galerkin method*, in: Recent developments in discontinuous Galerkin finite element methods for partial differential equations, Springer, 2014, pp. 149–180.

[7] L. F. Demkowicz, J. Gopalakrishnan, S. Nagaraj and P. Sepulveda, A spacetime DPG method for the Schrödinger equation, *SIAM J. Numer. Anal.* 55 (2017), 1740–1759.

[8] W. Dörfler, S. Findeisen and C. Wieners, Space-time discontinuous Galerkin discretizations for linear first-order hyperbolic evolution systems, *Comput. Methods Appl. Math.* 16 (2016), 409–428.

[9] M. Dumbser, M. Käser and E. F. Toro, An arbitrary high-order discontinuous Galerkin method for elastic waves on unstructured meshes – V. Local time stepping and p-adaptivity, *Geophys. J. Int.* 171 (2007), 695–717.

[10] H. Egger, F. Kretzschmar, S. M. Schnepp and T. Weiland, A space-time discontinuous Galerkin–Trefftz method for time dependent Maxwell's equations, *SIAM J. Sci. Comp.* 37 (2015), B689–B711.

[11] T. E. Ellis, L. F. Demkowicz, J. L. Chan and R. D. Moser, *Space-time DPG: Designing a method for massively parallel CFD*, 2014, ICES REPORT 14-32.

[12] K.-J. Engel and R. Nagel, *A short course on operator semigroups*, Universitext, Springer, New York, 2006.

[1] http://www.scc.kit.edu/dienste/bwUniCluster.php (last access June 18, 2018)

Acoustic Wave

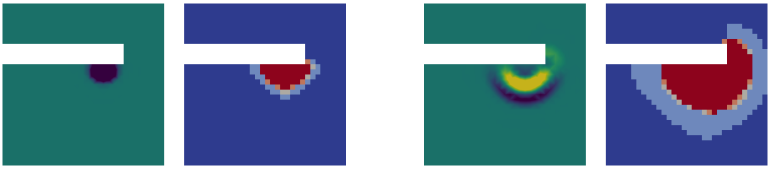

(a) $t = 0.0$ (b) $t = 0.6$

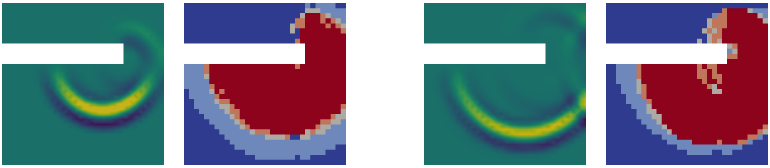

(c) $t = 1.2$ (d) $t = 1.8$

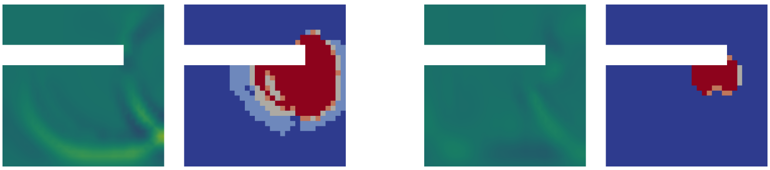

(e) $t = 2.4$ (f) $t = 3.0$

Elastic Wave

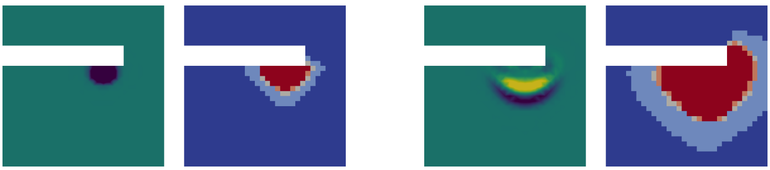

(g) $t = 0.0$ (h) $t = 0.6$

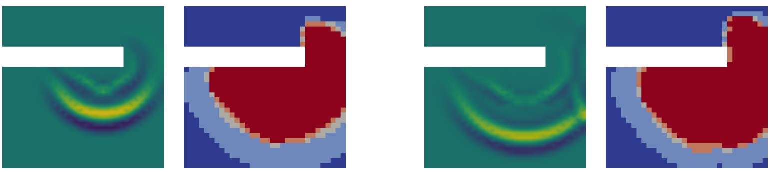

(i) $t = 1.2$ (j) $t = 1.8$

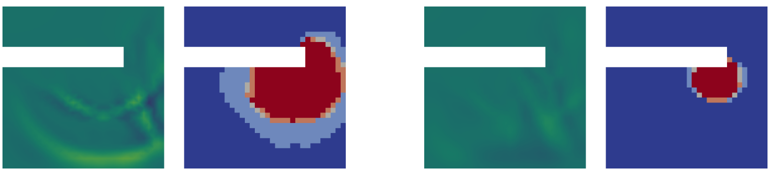

(k) $t = 2.4$ (l) $t = 3.0$

Figure 5. Acoustic and elastic waves: Velocity component v_2 and adaptive distribution of polynomial degrees.

[13] J. Ernesti, *Space-time methods for acoustic waves with applications to full waveform inversion*, Ph.D. thesis, Karlsruher Institut für Technologie (KIT), 2018.

[14] R. D. Falgout, S. Friedhoff, T. V. Kolev, S. P. MacLachlan and J. B. Schroder, Parallel time integration with multigrid, *SIAM J. Sci. Comput.* 36 (2014), C635–C661.

[15] M. J. Gander, *50 years of time parallel time integration*, Multiple Shooting and Time Domain Decomposition (T. Carraro, M. Geiger, S. Körkel and R. Rannacher, eds.), Springer, 2015.

[16] M. J. Gander, L. Halpern and F. Nataf, Optimal Schwarz waveform relaxation for the one dimensional wave equation, *SIAM J. Numer. Anal.* 41 (2003), 1643–1681.

[17] M. J. Gander and M. Neumüller, Analysis of a new space-time parallel multigrid algorithm for parabolic problems, *SIAM J. Sci. Comput.* 38 (2016), A2173–A2208.

[18] M. J. Gander and S. Vandewalle, Analysis of the parareal time-parallel time-integration method, *SIAM J. Sci. Comput.* 29 (2007), 556–578.

[19] J. S. Hesthaven and T. Warburton, *Nodal discontinuous Galerkin Methods*, Springer, 2008.

[20] M. Hochbruck, T. Pazur, A. Schulz, E. Thawinan and C. Wieners, Efficient time integration for discontinuous Galerkin approximations of linear wave equations, *ZAMM* 95 (2015), 237–259.

[21] S. Kestler, K. Steih and K. Urban, An efficient space-time adaptive wavelet Galerkin method for time-periodic parabolic partial differential equations, *Math. Comp.* 85 (2016), 1309–1333.

[22] U. Köcher and M. Bause, Variational space-time methods for the wave equation, *J. Sci. Comput.* 61 (2014), 424–453.

[23] F. Kretzschmar, A. Moiola, I. Perugia and S. M. Schnepp, A priori error analysis of space-time Trefftz discontinuous Galerkin methods for wave problems, *IMA J. Numer. Anal.* (2015), 1599–1635.

[24] U. Langer, S. E Moore and M. Neumüller, Space-time isogeometric analysis of parabolic evolution problems, *Comp. Meth. Appl. Mech. Engrg.* 306 (2016), 342–363.

[25] J.-L. Lions, Y. Maday and G. Turinici, A ”parareal” in time discretization of PDE's, *C. R. Acad. Sci. Paris, Ser. I* 332 (2001), 661–668.

[26] D. Maurer and C. Wieners, A parallel block LU decomposition method for distributed finite element matrices, *Parallel Comput.* 37 (2011), 742–758.

[27] ———, A scalable parallel factorization of finite element matrices with distributed Schur complements, *Numer. Linear Algebra Appl.* 23 (2016), 848–864.

[28] M. Neumüller and O. Steinbach, Refinement of flexible space-time finite element meshes and discontinuous Galerkin methods, *Comput. Vis. Sci.* 14 (2011), 189–205.

[29] ———, *A DG space-time domain decomposition method*, Domain Decomposition Methods in Science and Engineering XX, Springer, 2013, pp. 623–630.

[30] N. C. Nguyen, J. Peraire and B., High-order implicit hybridizable discontinuous Galerkin methods for acoustics and elastodynamics, *J. Comput. Phys.* 230 (2011), 3695–3718.

[31] S. Petersen, C. Farhat and R. Tezaur, A space-time discontinuous Galerkin method for the solution of the wave equation in the time domain, *Int. J. Numer. Meth. Engng.* 78 (2009), 275–295.

[32] M. Renardy and R. C. Rogers, *An introduction to partial differential equations. 2nd ed.*, New York, NY: Springer, 2004 (English).

[33] S. Rhebergen, B. Cockburn and J. J. W. van der Vegt, A space-time discontinuous Galerkin method for the incompressible Navier–Stokes equations, *J. Comput. Phys.* 233 (2013), 339–358.

[34] C. Schwab and R. Stevenson, Space-time adaptive wavelet methods for parabolic evolution problems, *Math. Comp.* 78 (2009), 1293–1318.

[35] R. Speck, D. Ruprecht, M. Emmett, M. Bolten and R. Krause, A space-time parallel solver for the three-dimensional heat equation, in: *Parallel Computing: Accelerating Computational Science and Engineering (CSE)* (M. Bader, A. Bode, H.-J. Bungartz, M. Gerndt, G. R. Joubert and F. J. Peters, eds.), Advances in Parallel Computing 25, pp. 263–272, IOS Press, 2014.

[36] O. Steinbach, Space-time finite element methods for parabolic problems, *Comput. Meth. Appl. Math.* 15 (2015), 551–566.

[37] O. Steinbach and H. Yang, Comparison of algebraic multigrid methods for an adaptive space-time finite-element discretization of the heat equation in 3D and 4D, *Numerical Linear Algebra with Applications* 25 (2018), e2143.

[38] J. J. W. van der Vegt and S. Rhebergen, hp-multigrid as smoother algorithm for higher order discontinuous Galerkin discretizations of advection dominated flows: Part I. Multilevel analysis, *J. Comput. Phys.* 231 (2012), 7537–7563.

[39] D. Wang, R. Tezaur and C. Farhat, A hybrid discontinuous in space and time Galerkin method for wave propagation problems, *Int. J. Numer. Meth. Engng* (2014).

Author information

Willy Dörfler, Institut für Angewandte und Numerische Mathematik, KIT, D-76128 Karlsruhe, Germany.
E-mail: `Willy.Doerfler@kit.edu`

Stefan Findeisen, Institut für Angewandte und Numerische Mathematik, KIT, D-76128 Karlsruhe, Germany.

Christian Wieners, Institut für Angewandte und Numerische Mathematik, KIT, D-76128 Karlsruhe, Germany.
E-mail: `Christian.Wieners@kit.edu`

Daniel Ziegler, Institut für Angewandte und Numerische Mathematik, KIT, D-76128 Karlsruhe, Germany.
E-mail: `Daniel.Ziegler@kit.edu`